Hydrogen atom in a magnetic field: Ghost orbits, catastrophes, and uniform semiclassical approximations

Jörg Main* and Günter Wunner
Institut für Theoretische Physik I, Ruhr-Universität Bochum, D-44780 Bochum, Germany
(Received 11 September 1996)

Applying closed-orbit theory to the recurrence spectra of the hydrogen atom in a magnetic field, one can interpret most, but not all, structures semiclassically in terms of closed classical orbits. In particular, conventional closed-orbit theory fails near bifurcations of orbits where semiclassical amplitudes exhibit unphysical divergences. Here we analyze the role of ghost orbits living in complex phase space. The ghosts can explain resonance structures in the spectra of the hydrogen atom in a magnetic field at positions where no real orbits exist. For three different types of catastrophes, viz. fold, cusp, and butterfly catastrophes, we construct uniform semiclassical approximations and demonstrate that these solutions are completely determined by classical parameters of the real orbits and complex ghosts. [S1050-2947(97)07002-9]

PACS number(s): 32.60.+i, 03.65.Sq, 05.45.+b, 32.70.Cs

I. INTRODUCTION

Rydberg atoms in external magnetic fields are nontrivial systems possessing a classically chaotic counterpart, with at least two nonseparable, strongly coupled degrees of freedom. Ever since the discovery of quasi-Landau type modulations in the spectra of barium [1] and hydrogen [2,3] atoms, and their interpretation in terms of classical periodic motion, atoms in magnetic fields have served as prototype systems for studying quantum manifestations of classical chaos in real physical systems (for reviews see [4–6]). As the corresponding classical dynamics of Rydberg atoms is chaotic, the quantitative description of their quantum features in terms of classical orbits was, and still is, a big challenge to theory as regards the development and application of semiclassical methods.

A decisive advance for a semiclassical interpretation of structures in the photoabsorption cross section was achieved by the development of *closed-orbit theory* [7,8]. The method allows, at least in low resolution, not only a simple interpretation but also a quantitative calculation of spectra in terms of few parameters of the set of closed classical orbits starting at and returning to the nucleus. Semiclassical results are in good agreement with experimental data, e.g., of the hydrogen atom [9].

Closed-orbit theory fails, however, at energies where orbits undergo bifurcations, i.e., where closed or periodic orbits are born or vanish. Bifurcation is a phenomenon typical of classical periodic orbits in chaotic systems with nonhyperbolic Hamiltonian dynamics, such as the hydrogen atom in magnetic fields, which undergoes a transition from regularity to chaotic dynamics with increasing energy. The bifurcation scheme of this system has been analyzed in [10,11]. Near bifurcations closed-orbit theory fails, the semiclassical formulas diverge and are singular exactly at the bifurcation points. Such ''catastrophes'' not only occur in closed-orbit theory but are well-known phenomena in various fields of physics, e.g., in semiclassical scattering theory [12,13], diffraction theory in optics [14], or periodic orbit theory [15]. Different kinds of catastrophes exist and are characterized by various forms of caustics of a bundle of lines (or, more specific, in physical systems a bundle of classical trajectories or light rays). A systematic mathematical classification and analysis of structurally stable caustics was achieved by the development of *catastrophe theory* [16].

The divergences in semiclassical theories can be removed by the construction of *uniform* semiclassical solutions [12,13]. Their calculation is generally not unique because the topological structure of the related catastrophe must be considered. Uniform semiclassical approximations have been constructed, e.g., for atomic and molecular scattering problems [12,13,17,18], photodetachment of H^- in parallel electric and magnetic fields [19], time-dependent wave-packet propagation [20], and for continuum Stark spectra [21]. In an application of periodic orbit theory to a kicked top [22] it was demonstrated that prebifurcation periodic *ghost orbits* exist, and are of importance in the semiclassical interpretation of that system.

It is the purpose of this paper to investigate the role of ghost orbits and their relation to catastrophes and uniform semiclassical approximations in more detail. As a specific system we study the hydrogen atom in a magnetic field and demonstrate that around the singular points of standard closed-orbit theory, i.e., at the bifurcations of orbits, uniform semiclassical approximations can be obtained from only a few parameters of closed orbits, provided the type of catastrophe is known, and not only real but also complex ghost orbits are considered. The paper is organized as follows: In Sec. II we discuss the classical dynamics and the continuation of closed orbits to complex phase space, i.e., the ghost orbits. In Sec. III we derive uniform semiclassical approximations for three different kinds of catastrophes. A discussion of results and concluding remarks follow in Secs. IV and V.

II. CLASSICAL DYNAMICS AND GHOST ORBITS

The basic equations for the calculation of classical trajectories and a periodic orbit search for the hydrogen atom in a

*Present address: Dept. of Chemistry, University of Southern California, Los Angeles, CA 90089.

magnetic field are given in many papers (see, e.g., [4]). Here we briefly review the main ideas only, and concentrate on the peculiarities of a complex continuation of phase space, the search for ghost orbits, and the calculation of the (complex) ghost orbit parameters.

The nonrelativistic Hamiltonian for the hydrogen atom in a magnetic field of strength B directed along the z axis has the well-known form [in atomic units, $\gamma = B/(2.35\times 10^5\ \mathrm{T})$]

$$H=\frac{1}{2}\mathbf{p}^2-\frac{1}{r}+\frac{1}{2}\gamma L_z+\frac{1}{8}\gamma^2\varrho^2=E. \tag{2.1}$$

The component of the angular momentum parallel to the field axis is conserved and we choose $L_z=m\hbar=0$ in all classical calculations.

A special feature of the Hamiltonian is its scaling property with respect to the magnetic-field strength. In scaled coordinates and momenta,

$$\tilde{\mathbf{r}}=\gamma^{2/3}\mathbf{r},\quad \tilde{\mathbf{p}}=\gamma^{-1/3}\mathbf{p},$$

the classical Hamiltonian assumes the form

$$\tilde{H}=\gamma^{-2/3}H=\frac{1}{2}\tilde{\mathbf{p}}^2-\frac{1}{\tilde{r}}+\frac{1}{8}\tilde{\varrho}^2=\tilde{E}. \tag{2.2}$$

The classical trajectories obtained from the scaled equations of motion do not depend on both energy and magnetic-field strength, but only on one parameter, the scaled energy $\tilde{E}=E\gamma^{-2/3}$. Note that the classical action scales as

$$S=2\pi\tilde{S}\gamma^{-1/3}. \tag{2.3}$$

The Coulomb singularity presents an obstacle to the numerical integration of the equations of motion that follow from the Hamiltonian (2.2). The way out of this problem is a transformation of time $t\mapsto\tau$, with $dt=2r\,d\tau$, called regularization [23], together with a coordinate transformation to semiparabolical coordinates

$$\mu=\sqrt{r+z},\quad \nu=\sqrt{r-z}. \tag{2.4}$$

These transformations lead to the regularized Hamiltonian

$$\mathcal{H}=\tfrac{1}{2}(p_\mu^2+p_\nu^2)-E(\mu^2+\nu^2)+\tfrac{1}{8}\gamma^2\mu^2\nu^2(\mu^2+\nu^2)=2, \tag{2.5}$$

from which we obtain Hamilton's equations of motion (the primes denote derivatives $d/d\tau$)

$$\mu'=p_\mu,\quad p_\mu'=2E\mu-\gamma^2(\mu^3\nu^2/2+\mu\nu^4/4),$$
$$\nu'=p_\nu,\quad p_\nu'=2E\nu-\gamma^2(\nu^3\mu^2/2+\nu\mu^4/4). \tag{2.6}$$

These equations are free of singularities, and were integrated numerically with the help of a high-order predictor-corrector multistep algorithm.

In a semiclassical approximation to photoabsorption spectra (see Sec. III) closed orbits, which start at and return to the nucleus, are of fundamental importance. The closed-orbit search can be formulated as finding roots (ϑ_i,τ_f) of the two equations

$$\mu(\vartheta_i,\tau_f)=\nu(\vartheta_i,\tau_f)=0 \tag{2.7}$$

when integrating Hamilton's equations (2.6) with the initial conditions (at $\tau=0$)

$$\mu(0)=0,\quad p_\mu(0)=2\cos(\vartheta_i/2)$$
$$\nu(0)=0,\quad p_\nu(0)=2\sin(\vartheta_i/2). \tag{2.8}$$

Here ϑ_i is the starting angle, i.e., the angle between the initial velocity of the electron and the field axis. Equation (2.7) can be solved numerically with the help of an iterative Newton algorithm, and its roots (ϑ_i,τ_f) are the *real* closed orbits [3,9] when all parameters are defined real.

The analytic structure of the equations of motion (2.6) allows a direct analytic continuation of the real phase space (μ,ν,p_μ,p_ν) to complex numbers. To search for complex closed orbits we choose the same initial conditions (2.8) but with complex starting angle ϑ_i, i.e., the momenta $p_\mu(0)$ and $p_\nu(0)$ become complex, but the condition $\mathcal{H}=2$ in Eq. (2.5) is still satisfied. With these complex initial conditions Hamilton's equations of motion (2.6) can be integrated numerically from $\tau=0$ to $\tau=\tau_f$. It should be noted that in general τ_f also must be chosen as a complex number to find ghost orbits as roots of Eq. (2.7). In this case we integrate trajectories along straight lines in the complex plane from $\tau=0$ to $\tau=\tau_f$, but the final parameters of ghost orbits such as the complex recurrence time

$$T=\int_0^{\tau_f}(\mu^2+\nu^2)\,d\tau \tag{2.9}$$

and the action

$$S=\int_0^{\tau_f}(p_\mu^2+p_\nu^2)\,d\tau \tag{2.10}$$

do not depend on any special choice of this path because of the analytic structure of the equations of motion. This is also true for the monodromy matrix $\mathbf{M}$, i.e., the stability matrix restricted to deviations perpendicular to a periodic orbit after period T. To be more specific, if $\delta q(0)$ is a small deviation perpendicular to the orbit in coordinate space at time $t=0$ and $\delta p(0)$ an initial deviation in momentum space, the corresponding deviations at time $t=T$ are related to the monodromy matrix [8], viz.

$$\begin{pmatrix}\delta q(T)\\ \delta p(T)\end{pmatrix}=\mathbf{M}\begin{pmatrix}\delta q(0)\\ \delta p(0)\end{pmatrix}=\begin{pmatrix}m_{11}&m_{12}\\ m_{21}&m_{22}\end{pmatrix}\begin{pmatrix}\delta q(0)\\ \delta p(0)\end{pmatrix}. \tag{2.11}$$

It is not our intention in this paper to carry out a complete search for all real and complex closed orbits. Rather, our attention will be focused on the occurrence of ghost orbits in the vicinity of bifurcations of real orbits, and we shall discuss three specific examples, viz. the saddle node bifurcation of orbit X_1, the period doubling of V_1^1, and a more complex bifurcation of the perpendicular orbit R_1. Shapes of orbits near these bifurcations are shown in Fig. 1. For the classification of closed orbits we adopt the nomenclature of [3], i.e., orbits R_μ^ν bifurcate from the motion perpendicular to the field

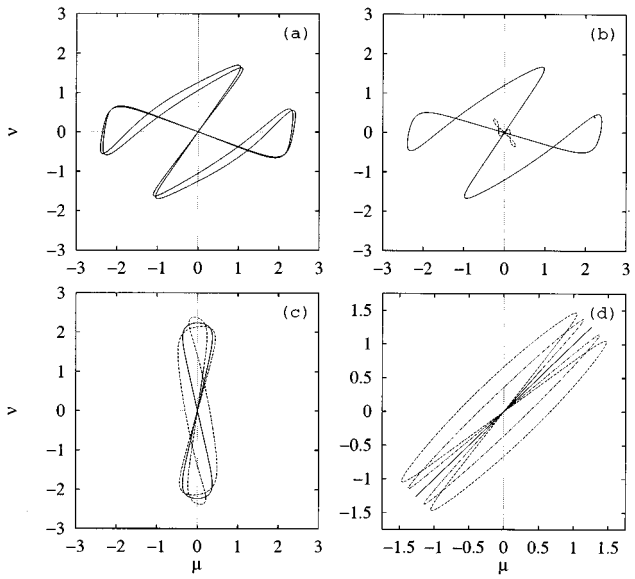

FIG. 1. Closed orbits (in semiparabolic coordinates μ,ν) at scaled energies near bifurcation points. (a) Orbits X_1^a and X_1^b at energy $\widetilde{E}=-0.11$. Both orbits are born in a saddle-node bifurcation at $\widetilde{E}_b=-0.115\,442\,16$. (b) Ghost orbit X_1 at energy $\widetilde{E}=-0.2$. Solid line: Reμ vs Reν. Dashed line: Imμ vs Imν. (c) Balloon orbit V_1^1 at energy $\widetilde{E}=-0.32$ (solid line) and orbit V_2^{2*} (dashed line) bifurcating in a period doubling at $\widetilde{E}_b=-0.342\,025\,8$. (d) Perpendicular orbit R_2 (solid line), orbit R_2^1 (dashed line), and orbit R_2^{1b} (dashed dotted line) at scaled energy $\widetilde{E}=-0.317$.

axis, V_μ^ν denotes orbits bifurcating directly from the motion parallel to the field, with higher-order bifurcations marked by an asterisk, and orbits X_μ are created ''out of nowhere,'' mostly in saddle-node bifurcations.

A. Saddle-node bifurcation of the orbit X_1

The first example we discuss in detail is the orbit X_1, which is created in a saddle-node bifurcation at scaled energy $\widetilde{E}_b=-0.115\,442\,16$ and with initial and final angles $\vartheta_i=1.2271$, $\vartheta_f=2.4232$ [10]. At higher energies ($\widetilde{E}>\widetilde{E}_b$) this orbit immediately splits up into two different real closed orbits (X_1^a and X_1^b) with slightly different shapes, examples of which are shown in Fig. 1(a) for energy $\widetilde{E}=-0.11$. With decreasing energy, both orbits are found to vanish exactly at the bifurcation point, and below the bifurcation energy ($\widetilde{E}<\widetilde{E}_b$) no real closed orbit with similar shape exists. However, the closed-orbit search extended to the complex continuation of phase space indeed reveals the existence of prebifurcation ghost orbits. For illustrational purposes the ghost orbit is presented in Fig. 1(b) at energy $\widetilde{E}=-0.2$. The real parts of semiparabolic coordinates (solid line) look similar to orbits found above the bifurcation energy [Fig. 1(a)] and the imaginary parts (dashed line) are usually relatively small. Note that the complex conjugate (ϑ_i^*,τ_f^*) of each ghost orbit is also a solution of Eq. (2.7), i.e., there exist two closed orbits above and below the bifurcation energy which are degenerate exactly at the bifurcation point.

For the construction of uniform semiclassical approximations in Sec. III some closed-orbit parameters, namely, the initial and final angles, the classical action, and the element m_{12} of the monodromy matrix, are of fundamental importance. The energy dependence of these parameters show characteristics around the bifurcation point which are related to the various types of bifurcations. In Fig. 2 we present the results for the saddle-node bifurcation of the orbits X_1^a and X_1^b. The energy dependence of the starting angles ϑ_i is given in Fig. 2(a). Both angles are real above the bifurcation en-

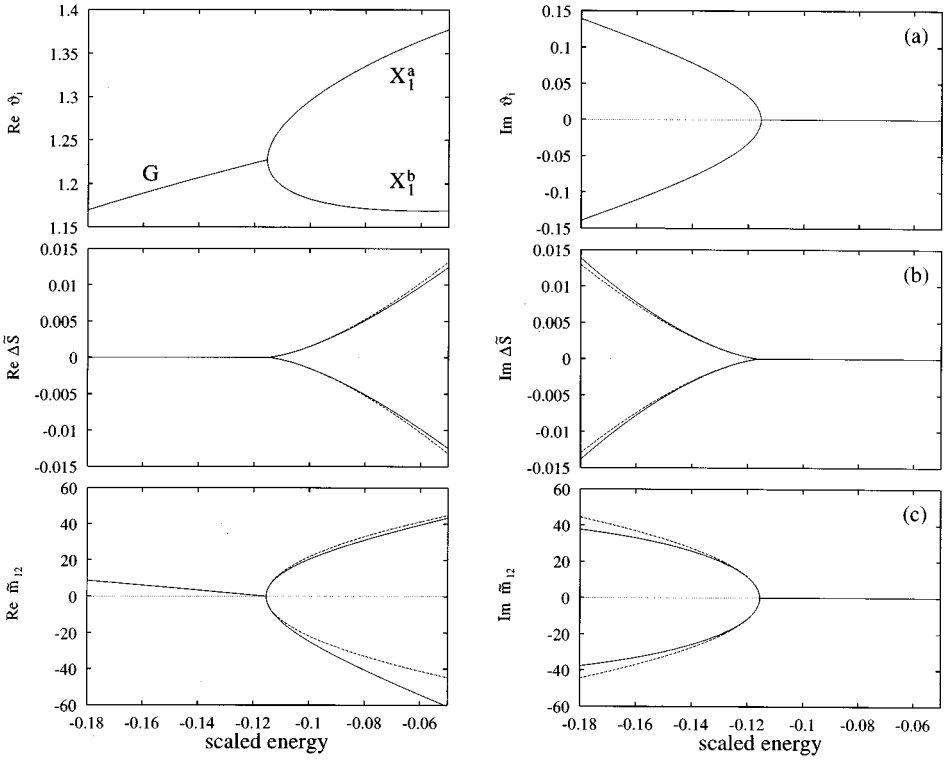

FIG. 2. (a) Real and imaginary part of starting angle ϑ_i for closed orbits around the saddle-node bifurcation of X_1 at scaled energy $\widetilde{E}_b=-0.115\,442\,16$. G: Complex ghost orbit. (b) Difference in scaled action $\Delta\widetilde{S}=\pm(\widetilde{S}_2-\widetilde{S}_1)/2$ with $\widetilde{S}_{1,2}$ the action of the two real and ghost orbits respectively. (c) Real and imaginary part of monodromy matrix element $\widetilde{m}_{12}$ for closed orbits around the saddle-node bifurcation of X_1. Dashed lines: Analytical fits (see text).

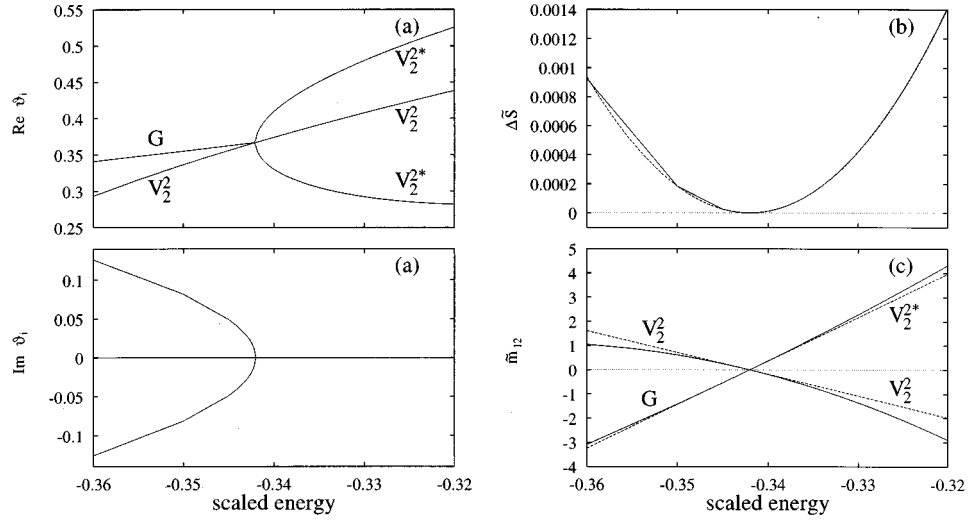

FIG. 3. (a) Real and imaginary part of starting angle ϑ_i for closed orbits around the period doubling bifurcation of V_1^1 at scaled energy $\widetilde{E}_b=-0.342\,025\,8$. G: Ghost orbit. (b) Difference $\Delta\widetilde{S}$ between the classical action of the (period doubled) balloon orbit V_2^2 and real and ghost orbits bifurcating from it. (c) Monodromy matrix element $\widetilde{m}_{12}$ of the balloon orbit V_2^2 and orbits bifurcating from it. Although the ghost orbit G lives in complex phase space its action and monodromy matrix element remain real. Dashed lines: Analytical fits (see text).

ergy, form a saddle at the bifurcation point, and become complex for the ghost orbits below the bifurcation energy. Figure 2(b) shows the deviation of the classical action from the mean value, $\Delta\widetilde{S}=\pm(\widetilde{S}_2-\widetilde{S}_1)/2$, where $\widetilde{S}_1$ and $\widetilde{S}_2$ are the classical actions of the orbits X_1^a and X_1^b. Close to bifurcation points the energy dependence of closed-orbit parameters can be approximated by analytical functions. For $\Delta\widetilde{S}$ we obtain

$$\Delta\widetilde{S}=\pm(\widetilde{\sigma}/2\pi)(\widetilde{E}-\widetilde{E}_b)^{3/2} \tag{2.12}$$

with $\widetilde{\sigma}=4.96$ [see the dashed line in Fig. 2(b)]. The monodromy matrix elements $\widetilde{m}_{12}$ of both orbits X_1^a and X_1^b vanish exactly at the bifurcation point, and can be approximated at $\widetilde{E}\approx\widetilde{E}_b$ by

$$\widetilde{m}_{12}=\pm\widetilde{M}(\widetilde{E}-\widetilde{E}_b)^{1/2} \tag{2.13}$$

with $\widetilde{M}=175$, as is illustrated by the solid and dashed lines in Fig. 2(c). Note that the behavior of ghost orbit parameters $\Delta\widetilde{S}$ and $\widetilde{m}_{12}$ at energies $\widetilde{E}<\widetilde{E}_b$ is simply the analytic continuation of Eqs. (2.12) and (2.13). Vice versa, a study of the behavior of solely the real orbit parameters already suggests the existence of ghost orbits with properties revealed by the more sophisticated search for ghost orbits in complex phase space.

B. Period doubling of the balloon orbit V_1^1

The second example of a bifurcation we study in detail is the period doubling of the balloon orbit V_1^1 at scaled energy $\widetilde{E}_b=-0.342\,025\,8$. The balloon orbit itself is already created at lower energy $\widetilde{E}=-0.3913$ in a bifurcation from the orbit parallel to the field [10]. A special feature of its shape is the symmetry in the initial and final angle, i.e., $\vartheta_i=\vartheta_f$. It exists below and above the period-doubling energy without any spectacular change of this shape. Above the period-doubling energy a new orbit V_2^{2*} which breaks this symmetry ($\vartheta_i\neq\vartheta_f$) separates from V_1^1 and is closed roughly after two times the period of V_1^1. Examples of the shapes of the balloon orbit and its period-doubling bifurcation V_2^{2*} are shown in Fig. 1(c).

We searched for complex orbits in the vicinity of this bifurcation and found a ghost orbit (and its complex conjugate) at energies below the bifurcation. The energy dependence of closed-orbit parameters ϑ_i, $\Delta\widetilde{S}$, and $\widetilde{m}_{12}$ is presented in Fig. 3. There exist three real starting angles ϑ_i at $\widetilde{E}>\widetilde{E}_b$, and one real and two complex angles at $\widetilde{E}<\widetilde{E}_b$ [see Fig. 3(a)]. The classical action and the monodromy matrix element m_{12} show a strange and unexpected behavior in the following sense. Although the ghost orbit is embedded in complex phase space, these parameters remain exactly real even far away from the bifurcation point. The difference $\Delta\widetilde{S}$ in action between orbits V_2^{2*} and V_2^2 is approximately given by a parabola

$$\Delta\widetilde{S}=(\widetilde{\sigma}/2\pi)(\widetilde{E}-\widetilde{E}_b)^2 \tag{2.14}$$

with $\widetilde{\sigma}=18.27$ [see Fig. 3(b)], and the monodromy matrix elements $\widetilde{m}_{12}$ of orbits V_2^2 and V_2^{2*} are approximately linear functions of the energy distance from the bifurcation point

$$\widetilde{m}_{12}=-\widetilde{M}(\widetilde{E}-\widetilde{E}_b)\quad(\text{orbit } V_2^2),$$

$$\widetilde{m}_{12}=2\widetilde{M}(\widetilde{E}-\widetilde{E}_b)\quad(\text{orbit } V_2^{2*} \text{ and ghost}) \tag{2.15}$$

with $\widetilde{M}=91$ [see Fig. 3(c)]. Note that, as for the saddle-node bifurcation (Sec. II A), the energy dependence of ghost orbit parameters $\Delta\widetilde{S}$ and $\widetilde{m}_{12}$ is simply the analytic continuation of Eqs. (2.14) and (2.15) for the real orbit V_2^{2*}, i.e., the parameters remain real at $\widetilde{E}<\widetilde{E}_b$.

C. Bifurcation of the orbit perpendicular to the field

In this section we investigate real and ghost orbits related to the period doubling of the perpendicular orbit R_1. This third example of closed-orbit bifurcations is more complicated because various orbits with similar periods undergo two different elementary types of bifurcations at nearly the same energy. The shapes of the real orbits at scaled energy $\widetilde{E}=-0.317$ are plotted in Fig. 1(d), R_1 (solid line $\mu=\nu$) is the orbit perpendicular to the magnetic-field axis, and the dashed and dashed-dotted lines represent the orbits R_2^1 and R_2^{1b} (''Pacmen'' in [10]).

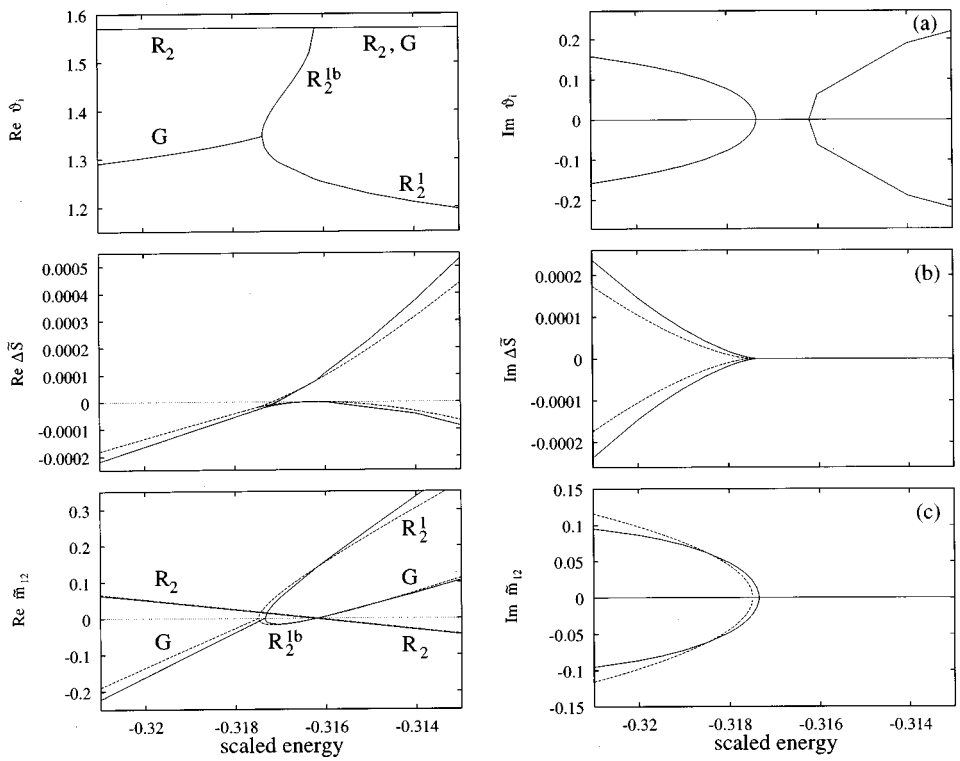

FIG. 4. (a) Real and imaginary part of starting angle ϑ_i for closed orbits related to the bifurcating scenario of the (period doubled) perpendicular orbit R_2. (b) Difference $\Delta\widetilde{S}$ between the classical action of the (period doubled) perpendicular orbit R_2 and real and ghost orbits bifurcating from it. (c) Monodromy matrix element $\widetilde{m}_{12}$ of the perpendicular orbit R_2 and orbits bifurcating from it. Dashed lines: Analytical fits (see text).

The structure of bifurcations and the appearance of ghost orbits can be seen clearly in the energy dependence of the starting angles ϑ_i in Fig. 4(a). Orbits R_2^1 and R_2^{1b} are created in a saddle-node bifurcation at $\widetilde{E}_b^{(1)}=-0.317\,353\,45$, $\vartheta_i=1.3465$. Below the bifurcation energy we find (in analogy to the saddle-node bifurcation discussed in Sec. II A) an associated ghost orbit and its complex conjugate. Orbit R_2^{1b} is real only in a very short energy interval ($\Delta\widetilde{E}\approx 0.001$), and is then involved in the next bifurcation at $\widetilde{E}_b^{(2)}=-0.316\,185\,37$, $\vartheta_i=\pi/2$. This is the period-doubling bifurcation of the perpendicular orbit R_1, which exists at all energies [$\vartheta_i=\pi/2$ in Fig. 4(a)]. The period doubling is similar to the bifurcation of V_1^1 discussed in Sec. II B but with a reversed energy dependence. The real orbit R_2^{1b} separates from R_1 at energies *below* the bifurcation point, i.e., a real orbit vanishes with increasing energy. Consequently associated ghost orbits are expected at energies *above* the bifurcation, i.e., $\widetilde{E}>\widetilde{E}_b^{(2)}$, and indeed such ''postbifurcation'' ghosts have been found. Its complex starting angles are also shown in Fig. 4(a).

The energy dependence of scaled actions, or, more precisely, the difference $\Delta\widetilde{S}$ with respect to the action of the period-doubled perpendicular orbit R_2, is presented in Fig. 4(b) (solid lines), and the graph for the monodromy matrix element $\widetilde{m}_{12}$ is given in Fig. 4(c). It can be seen that the actions and the monodromy matrix elements of the ghost orbits related to the saddle-node bifurcation of R_2^1 become complex at $\widetilde{E}<\widetilde{E}_b^{(1)}$, while these parameters remain real for the postbifurcation ghosts at $\widetilde{E}>\widetilde{E}_b^{(2)}$. The two bifurcations are so closely adjacent that neither Eqs. (2.12) and (2.13), for the saddle-node bifurcation, nor Eqs. (2.14) and (2.15), for the period doubling, yield a reasonable approximation to $\Delta\widetilde{S}(\widetilde{E})$ and $\widetilde{m}_{12}(\widetilde{E})$ in the neighborhood of the bifurcations. However, both functions can be fitted well by the more complicated formulas

$$\Delta\widetilde{S}=\frac{k}{2\pi}\left(\widetilde{\sigma}(\widetilde{E}-\widetilde{E}_b^{(2)})+\tfrac{2}{3}\{1\pm[\widetilde{\sigma}(\widetilde{E}-\widetilde{E}_b^{(2)})+1]^{3/2}\}\right) \tag{2.16}$$

and

$$\widetilde{m}_{12}=-\widetilde{M}(\widetilde{E}-\widetilde{E}_b^{(2)}) \quad (\text{orbit } R_2)$$

$$\widetilde{m}_{12}=4\widetilde{M}(\widetilde{E}-\widetilde{E}_b^{(2)})+\frac{4\widetilde{M}}{\widetilde{\sigma}}[1\pm\sqrt{\widetilde{\sigma}(\widetilde{E}-\widetilde{E}_b^{(2)})+1}] \quad (R_2^1,\ R_2^{1b},\ \text{and ghosts}) \tag{2.17}$$

with $k=3.768\times10^{-4}$, $\widetilde{\sigma}=763.6$, and $\widetilde{M}=13.52$ [see the dashed lines in Figs. 4(b) and 4(c)]. Note that Eqs. (2.16) and (2.17) describe the complete scenario for the real and the ghost orbits including both the saddle-node and period-doubling bifurcations. We also mention that orbits with angles $\vartheta_i\neq\vartheta_f$ have to be counted twice because they correspond to different orbits when traversed in either direction, and therefore a total number of *five* closed orbits, including ghosts, is considered here in the bifurcaton scenario around the period doubling of the perpendicular orbit.

III. UNIFORM SEMICLASSICAL APPROXIMATIONS

In this section we investigate in which way bifurcations of classical orbits and the existence of ghost orbits manifest themselves in quantum mechanics. More specifically we shall study the related quantum effects that can be observed in the photoabsorption spectra of the hydrogen atom in magnetic fields. The link between classical trajectories and pho-

toabsorption spectra is established by a semiclassical *closed-orbit* theory [7,8]. In its original version, the element m_{12} of the monodromy matrix appears in the denominator of semiclassical expressions, and therefore the theory breaks down at the bifurcation points of orbits, where $m_{12}=0$. In the following we briefly review the general ideas of closed-orbit theory and then derive uniform semiclassical approximations valid around the bifurcation energies of closed-orbit bifurcations. We demonstrate that the uniform solutions are directly related to various types of *catastrophes* [16] formed by the bundle of returning trajectories and study three examples, namely, the fold, cusp, and butterfly catastrophe. The final uniform expressions are free of singularities. In particular, the analysis will reveal the importance of classical ghost orbits to quantum photoabsorption spectra.

A. The ansatz

The rationale of the semiclassical description of photoabsorption by atoms in strong magnetic fields is the following: An electron in a low-lying initial state $|\psi_i\rangle$ is excited to a Rydberg state, or a continuum state above the ionization threshold. One finds a distance r_0 from the nucleus where the semiclassical description of the wave functions becomes a good approximation, but the Lorentz forces are still negligibly small compared to the Coulomb attraction forces. Beyond r_0, the outgoing Coulomb wave describing the electron in the final state is propagated along classical trajectories. These trajectories obey the complete classical dynamics of the Hamiltonian (2.1), i.e., with the effects of the magnetic field included. The latter become important at large distances from the nucleus, and the combined action of the magnetic-field forces and the Coulomb forces may cause trajectories to return to the nucleus. The returning waves interfere with the initial state in the dipole matrix element, and this interference gives rise to characteristic modulations in the photoabsorption cross section. Consequently, the semiclassical expression for the oscillator strength is found to be composed of two parts, a smoothly varying continuous background f^0 related to the initially excited *outgoing* Coulomb wave, and an oscillatory part from the contributions of all *returning* waves $\psi_m^{\mathrm{ret},k}$ related to closed orbits k (m designates the conserved magnetic quantum number)

$$f=f^0+\sum_{\mathrm{cl.o.}k} f_k^{\mathrm{osc}}, \tag{3.1}$$

with

$$f_k^{\mathrm{osc}}=-\frac{2}{\pi}(E-E_i)\mathrm{Im}\langle\psi_i|D|\psi_m^{\mathrm{ret},k}\rangle. \tag{3.2}$$

The derivation of the semiclassical wave function has been described in detail in the literature (see, e.g., [7–9]). Here we only recapitulate the essential points that are necessary to an understanding of what follows. The basic observation is that in the vicinity of the nucleus the orbits behave like regular Keplerian orbits, and every closed orbit (returning exactly to the nucleus at an angle ϑ_f with respect to the z axis) will be surrounded by an ensemble of similar, almost-closed orbits, which approach the nucleus at the same angle ϑ_f, but swing by the nucleus. For a given point (r,ϑ) in the neighborhood of the nucleus, one can find an almost-closed orbit (associated with a given closed orbit k) that passes through (r,ϑ). The almost-closed orbit contributes to the semiclassical wave function at (r,ϑ) with two terms, one belonging to the ''incoming'' and one belonging to the ''outgoing'' trajectory along the almost-closed orbit [passage through (r,ϑ) before or after the perihelion, respectively]

$$\psi_m^{\mathrm{ret},k}(r,\vartheta)=-\sqrt{2\pi\sin\vartheta_i}\,\mathcal{Y}_m(\vartheta_i)\times\sum_{\lambda=\mathrm{out,in}}\frac{\exp\left\{i\left[S^{\lambda,k}(r,\vartheta)-\frac{\pi}{2}\mu^{\lambda,k}+\frac{\pi}{4}\right]\right\}}{\sqrt{|J^{\lambda,k}(t,\vartheta_i)|}}. \tag{3.3}$$

Here ϑ_i is the starting angle of the closed orbit, and

$$S^{\lambda,k}(r,\vartheta)=S_m^k+\Delta S^{\lambda,k}(r,\vartheta), \tag{3.4}$$

$$\mu^{\lambda,k}=\mu^k+\Delta\mu^{\lambda,k} \tag{3.5}$$

(λ = out, in) are the classical actions and Maslov indices of the incoming and outgoing trajectory, respectively, where

$$S_m^k=\oint_{\mathrm{cl.o.}k}(p_\mu d\mu+p_\nu d\nu)+m\left(\frac{1}{2}\gamma T_k+\pi n_{z,k}\right) \tag{3.6}$$

denotes the classical action of the exactly closed orbit k including the action of the separable φ motion. In Eq. (3.6), T_k is the recurrence time, and $n_{z,k}$ the total number of crossings of the orbit k with the z axis. The Maslov index μ^k counts the total number of caustics along the closed orbit, and $\Delta S^{\lambda,k}(r,\vartheta)$ and $\Delta\mu^{\lambda,k}$ represent the differences of the actions and Maslov indices of the incoming and outgoing trajectory at the given point (r,ϑ) relative to the exactly closed orbit k. The quantity $J^{\lambda,k}$ in Eq. (3.3) is the Jacobi determinant of the incoming and outgoing trajectory,

$$J^{\lambda,k}(t,\vartheta_i)=r\sin\vartheta\det\left(\frac{\partial(\mu,\nu)}{\partial(\tau,\vartheta_i)}\right)^{\lambda,k}. \tag{3.7}$$

The angular function $\mathcal{Y}_m(\vartheta)$ in Eq. (3.3) can be expressed in terms of the matrix elements of the dipole operator with the initial state $|\psi_i\rangle$ and spherical harmonics (see Appendix A).

The wave function (3.3) is the starting point for our construction of uniform semiclassical solutions. At values of r where the semiclassical approximation is valid but the effects of the magnetic field can still be neglected, the semiclassical returning wave (3.3) must be expandable in the basis of the exact quantum-mechanical Coulomb wave functions. Taking for the latter their form at $E\approx 0$ we can write

$$\psi_m^{\mathrm{ret},k}(r,\vartheta)=\sum_{\ell=|m|}^{\infty}c_{\ell m}\sqrt{2/r}\,\mathrm{J}_{2\ell+1}(\sqrt{8r})Y_{\ell m}(\vartheta,0), \tag{3.8}$$

where the expansion coefficients $c_{\ell m}$ can be determined from

$$
\begin{aligned}
c_{\ell m}\sqrt{2/r}\mathrm{J}_{2\ell+1}(\sqrt{8r}) &\underset{r\to\infty}{\sim} c_{\ell m} \\
&\times 2^{1/4}\pi^{-1/2}r^{-3/4}(-1)^{\ell}\cos\left(\sqrt{8r}-\frac{3}{4}\pi\right) \\
&= 2\pi\int_0^{\pi}\psi_m^{\mathrm{ret},k}(r,\vartheta)Y_{\ell m}(\vartheta,0)\sin\vartheta\, d\vartheta \\
&\approx -(2\pi)^{3/2}\sqrt{\sin\vartheta_i\sin\vartheta_f}\,\mathcal{Y}_m(\vartheta_i)Y_{\ell m}(\vartheta_f,0) \\
&\times\exp\left(i\left[S_m^k-\frac{\pi}{2}\mu^k+\frac{\pi}{4}\right]\right) \\
&\times\sum_{\lambda=\mathrm{out,in}}\int_0^{\pi}\frac{\exp\left\{i\left[\Delta S^{\lambda,k}(r,\vartheta)-\frac{\pi}{2}\Delta\mu^{\lambda,k}\right]\right\}}{\left[r\left|\det\left(\frac{\partial(\mu,\nu)}{\partial(\tau,\vartheta_i)}\right)^{\lambda,k}\right|d\vartheta\right]^{1/2}}d\vartheta.
\end{aligned}
\tag{3.9}
$$

In Eq. (3.9) we have exploited the asymptotic form of the Bessel function, and the fact that the phase integral has its main contribution around the angle $\vartheta\approx\vartheta_f$ of the returning orbit, and that spherical harmonics with low-ℓ quantum numbers are smooth functions of ϑ. The form (3.8) is correct, in particular, in the region of the initial state, where the dipole matrix element has to be evaluated. Therefore we can insert Eq. (3.8) into Eq. (3.2), and obtain

$$
\begin{aligned}
f_k^{\mathrm{osc}} &= 2(E-E_i)\sqrt{\sin\vartheta_i\sin\vartheta_f}\,\mathcal{Y}_m(\vartheta_i)\mathcal{Y}_m(\vartheta_f) \\
&\times\mathrm{Im}\left\{\mathcal{A}\,\exp\left(i\left[S_m^k-\frac{\pi}{2}\mu^k+\frac{\pi}{4}\right]\right)\right\},
\end{aligned}
\tag{3.10}
$$

where the complex amplitude $\mathcal{A}$ is defined by

$$
\begin{aligned}
I(r) &\equiv \sum_{\lambda=\mathrm{out,in}}\int_0^{\pi}\frac{\exp\left\{i\left[\Delta S^{\lambda,k}(r,\vartheta)-\frac{\pi}{2}\Delta\mu^{\lambda,k}\right]\right\}}{\left[\left|\det\left(\frac{\partial(\mu,\nu)}{\partial(\tau,\vartheta_i)}\right)^{\lambda,k}\right|\right]^{1/2}}d\vartheta \\
&= \mathcal{A}\frac{\cos\left(\sqrt{8r}-\frac{3}{4}\pi\right)}{2\pi(2r)^{1/4}}
\end{aligned}
\tag{3.11}
$$

(Eq. (3.9) guarantees that the quantity $I(r)$ will always factorize in this form). Thus $\mathcal{A}$ can be determined by evaluating $I(r)$ at some value of r where, again, the semiclassical approximation is valid but magnetic-field effects are still negligible.

Equation (3.11) is the basis for the subsequent uniform approximations of the amplitude $\mathcal{A}$. The decisive quantities entering into $\mathcal{A}$ are ΔS, $\Delta\mu$, and the Jacobi matrix in the neighborhood of a returning (exactly closed) orbit. In the case of bifurcations, i.e., catastrophes, the behavior of these quantities differs significantly from that in the standard situation of isolated returning orbits, as will become evident in the following sections.

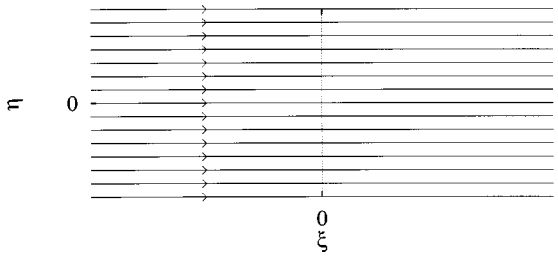

FIG. 5. Returning orbits close to the nucleus in the standard situation (monodromy matrix element $m_{12}\neq 0$) in rotated semiparabolic coordinates (ξ,η). Neighboring orbits are straight lines parallel to the ξ axis.

B. The standard situation: Isolated returning orbits

For completeness, and illustrative purposes, we start our discussion with the standard situation of nonbifurcating isolated returning orbits. We pick some closed orbit k, and will drop the index k for simplicity in what follows. In semiparabolic coordinates the returning trajectories are straight lines in the vicinity of the origin, inclined at an angle $\vartheta_f/2$ with respect to the μ axis. It is most convenient to introduce the rotated semiparabolic coordinates

$$
\xi=\mu\cos\frac{\vartheta_f}{2}+\nu\sin\frac{\vartheta_f}{2}=\sqrt{2r}\cos\frac{\vartheta-\vartheta_f}{2},
\tag{3.12}
$$

$$
\eta=\nu\cos\frac{\vartheta_f}{2}-\mu\sin\frac{\vartheta_f}{2}=\sqrt{2r}\sin\frac{\vartheta-\vartheta_f}{2},
\tag{3.13}
$$

where the ξ and η axes are now parallel and perpendicular to the returning orbit (see Fig. 5). All orbits satisfy the Hamilton-Jacobi equations

$$
p_\xi=\frac{\partial S}{\partial\xi}=2,\quad p_\eta=\frac{\partial S}{\partial\eta}=0.
\tag{3.14}
$$

The central returning (i.e., exactly closed) orbit is given by $\eta(\xi)=0$, while for the neighboring trajectories we have

$$
\eta(\xi)=m_{12}\Delta\vartheta_i,
\tag{3.15}
$$

where m_{12} is an element of the monodromy matrix, and $\Delta\vartheta_i$ is the deviation of the starting angle of the neighboring trajectory. We immediately obtain

$$
\begin{aligned}
\Delta S^{\lambda}(r,\vartheta) &= \pm 2|\xi| = \pm\sqrt{8r}\cos\frac{\vartheta-\vartheta_f}{2} \\
&= \pm[\sqrt{8r}-\sqrt{r/8}(\vartheta-\vartheta_f)^2],\quad \vartheta\approx\vartheta_f
\end{aligned}
\tag{3.16}
$$

$$
\det\left(\frac{\partial(\mu,\nu)}{\partial(\tau,\vartheta_i)}\right)^{\lambda}=\det\left(\frac{\partial(\xi,\eta)}{\partial(\tau,\vartheta_i)}\right)^{\lambda}=2\,m_{12}.
\tag{3.17}
$$

The Maslov index increases by 2 when the orbit passes the origin, i.e., the Maslov indices of the incoming and outgoing trajectory differ by

$$
\Delta\mu^{\lambda}=\pm 1.
\tag{3.18}
$$

Inserting Eqs. (3.16) to (3.18) into Eq. (3.11) we obtain (with the integration range of the stationary phase integral formally extended to $\pm\infty$)

$$I(r)=\left[\frac{2}{|m_{12}|}\right]^{1/2}\int_{-\infty}^{+\infty}\sin[\sqrt{8r}-\sqrt{r/8}(\vartheta-\vartheta_f)^2]d\vartheta$$

$$=\sqrt{\pi}2^{5/4}r^{-1/4}\frac{1}{\sqrt{|m_{12}|}}\cos\left(\sqrt{8r}-\frac{3}{4}\pi\right), \tag{3.19}$$

$$\Rightarrow \mathcal{A}=2(2\pi)^{3/2}\frac{1}{\sqrt{|m_{12}|}}. \tag{3.20}$$

The contribution of a nonbifurcating isolated returning orbit to the oscillator strength then reads (with the scaled monodromy matrix element $\widetilde{m}_{12}=\gamma^{1/3}m_{12}$)

$$f^{\rm osc}=2(E-E_i)\sqrt{\sin\vartheta_i\sin\vartheta_f}\mathcal{Y}_m(\vartheta_i)\mathcal{Y}_m(\vartheta_f)2(2\pi)^{3/2}\gamma^{1/6}$$

$$\times\frac{1}{\sqrt{|\widetilde{m}_{12}|}}\sin\left(S_m^0-\frac{\pi}{2}\mu^0+\frac{\pi}{4}\right). \tag{3.21}$$

This is exactly the result of conventional *closed-orbit* theory [7,8]. Obviously the oscillator strength diverges, i.e., conventional closed-orbit theory fails, at bifurcations of orbits, where $\widetilde{m}_{12}=0$. The reason for the occurrence of the divergence is that, in such a case, Eq. (3.15) does not correctly represent the behavior in the neighborhood of the central returning orbit. Thus the decisive point in the construction of a uniform semiclassical approximation in the vicinity of bifurcating points is an adequate expansion of Eq. (3.15) to higher orders in $\Delta\vartheta_i$. The order of the expansion required depends on the type of catastrophe, and therefore each case has to be treated separately. We shall investigate the fold, cusp, and butterfly catastrophes.

C. The fold catastrophe

An example for the occurrence of a fold catastophe in the hydrogen atom in a magnetic field is the creation of the closed orbit X_1 through a saddle-node bifurcation at the scaled energy $\widetilde{E}_b=-0.115\,442\,16$ discussed in Sec. II A. The family of corresponding returning orbits satisfy the Hamilton-Jacobi equations (in rotated semiparabolic coordinates, with $p_\xi=\partial S/\partial\xi$ and $p_\eta=\partial S/\partial\eta$)

$$cp_\eta^2+p_\xi[\xi p_\eta-p_\xi(\eta-\eta_0)]=0,$$

$$p_\xi^2+p_\eta^2=4 \tag{3.22}$$

from which we obtain (with $p_\eta/p_\xi\approx a\Delta\vartheta_i$)

$$\eta(\xi)=\eta_0+a^2c(\Delta\vartheta_i)^2+a(\Delta\vartheta_i)\xi. \tag{3.23}$$

Here η_0, a, and c are constants which will be specified later. The fold is illustrated in Fig. 6. At any point (ξ,η) Eq. (3.23) is a quadratic equation in $\Delta\vartheta_i$, with the discriminant

$$D=\frac{1}{(2ac)^2}\{\xi^2+4c(\eta-\eta_0)\}. \tag{3.24}$$

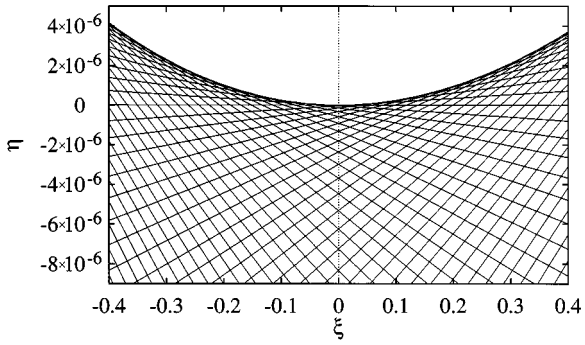

FIG. 6. Fold catastrophe of returning orbits (in rotated semiparabolic coordinates) related to the saddle-node bifurcation of orbit X_1 at bifurcation energy $\widetilde{E}_b=-0.115\,442\,16$.

If $D>0$ there exist two real solutions for $\Delta\vartheta_i$, i.e., two orbits return to these points, but no orbit returns to these points if $D<0$. The border line belonging to $D=0$ between the allowed and forbidden area is a caustic which has the shape of a parabola (see Fig. 6). The Hamilton-Jacobi equations (3.22) of the fold can be solved analytically. However, in the following derivations it is more convenient to use an approximate solution valid in the neighborhood of the central returning orbit

$$\Delta S^\lambda(r,\vartheta)=\pm\left[\sqrt{8r}-\eta_0(\vartheta-\vartheta_f)-\frac{c}{12}(\vartheta-\vartheta_f)^3\right],$$

$$\vartheta\approx\vartheta_f. \tag{3.25}$$

The determinant in the denominator of Eq. (3.11) is found to be given by

$$\det\left(\frac{\partial(\mu,\nu)}{\partial(\tau,\vartheta_i)}\right)^\lambda=\det\left(\frac{\partial(\xi,\eta)}{\partial(\tau,\vartheta_i)}\right)^\lambda$$

$$=\pm 2a\sqrt{\xi^2+4c(\eta-\eta_0)}\underset{r\gg 0}{\sim}$$

$$\pm a\sqrt{8r},\quad \vartheta\approx\vartheta_f \tag{3.26}$$

i.e., in the direction of the returning orbit it exhibits the behavior of a focus of orbits at the origin. This focus causes an additional increase of the Maslov index of outgoing trajectories; i.e., we have

$$\Delta\mu^{\rm out}=+2,\quad \Delta\mu^{\rm in}=-1. \tag{3.27}$$

We now insert Eqs. (3.25), (3.26), and (3.27) into Eq. (3.11). Extending formally again the integration range of the stationary phase integral to $\pm\infty$, we can express the integral in terms of the Airy function [26]:

$$I(r)=2^{1/4}r^{-1/4}|a|^{-1/2}\times\exp\left(-i\frac{\pi}{4}\right)\int_{-\infty}^{+\infty}\cos\left(\sqrt{8r}-\frac{3}{4}\pi-\eta_0(\vartheta-\vartheta_f)-\frac{c}{12}(\vartheta-\vartheta_f)^3\right)d\vartheta$$

$$=2^{1/4}r^{-1/4}|a|^{-1/2}\exp\left(-i\frac{\pi}{4}\right)\cos\left(\sqrt{8r}-\frac{3}{4}\pi\right)\times 2\pi(4/c)^{1/3}\mathrm{Ai}((4/c)^{1/3}\eta_0) \tag{3.28}$$

$$\Rightarrow\mathcal{A}=2^{5/2}\pi^2|a|^{-1/2}\times\exp\left(-i\frac{\pi}{4}\right)(4/c)^{1/3}\mathrm{Ai}((4/c)^{1/3}\eta_0). \tag{3.29}$$

After inserting the amplitude $\mathcal{A}$ into Eq. (3.10), the contribution of a fold catastrophe to the total semiclassical oscillator strength (3.1) reads

$$f^{\mathrm{osc}}=2(E-E_i)\sqrt{\sin\vartheta_i\sin\vartheta_f}\,\mathcal{Y}_m(\vartheta_i)\mathcal{Y}_m(\vartheta_f)2^{5/2}\times|a|^{-1/2}(4/c)^{1/3}\mathrm{Ai}((4/c)^{1/3}\eta_0)\sin\left(S_m^0-\frac{\pi}{2}\mu^0\right). \tag{3.30}$$

In Eq. (3.30) the parameters a, c, and η_0 are still undetermined. In the following we demonstrate that these parameters are directly related to closed classical trajectories. As can be seen from Eq. (3.24) no orbit returns to the origin ($\xi=\eta=0$) for $c\,\eta_0>0$ while two closed orbits exist for $c\,\eta_0<0$, i.e., at energies above the bifurcation energy. In the limit $c\,\eta_0\ll 0$, therefore, Eq. (3.30) should lead to the result of the standard situation (Eq. 3.21), applied to the two closed orbits. Taking the asymptotic forms of the Airy function (see Appendix B 1) in the limit $c\,\eta_0\ll 0$ we obtain from Eq. (3.30)

$$f^{\mathrm{osc}}=2(E-E_i)\sqrt{\sin\vartheta_i\sin\vartheta_f}\,\mathcal{Y}_m(\vartheta_i)\mathcal{Y}_m(\vartheta_f)2^{3/2}\pi^{-1/2}\times|a|^{-1/2}(-c\,\eta_0/4)^{-1/4}\times\left[\sin\left(S_m^0-\frac{2}{3}\sqrt{-4\,\eta_0^3/c}-\frac{\pi}{2}\mu^0+\frac{\pi}{4}\right)+\sin\left(S_m^0+\frac{2}{3}\sqrt{-4\,\eta_0^3/c}-\frac{\pi}{2}(\mu^0+1)+\frac{\pi}{4}\right)\right]. \tag{3.31}$$

Comparing this expression with Eq. (3.21) we can identify the contributions of two closed orbits with the Maslov indices μ^0 and μ^0+1. The classical actions S and monodromy matrix elements m_{12} of these orbits, expressed in terms of the parameters a, c, and η_0 in Eq. (3.31), must be identical to those obtained directly from classical trajectory calculations (see Sec. II A), from which we find the relations

$$S=S_m^0\mp\tfrac{2}{3}\sqrt{-4\,\eta_0^3/c}\equiv S_m^0\mp\gamma^{-1/3}\widetilde{\sigma}(\widetilde{E}-\widetilde{E}_b)^{3/2}, \tag{3.32}$$

$$m_{12}=\pm 2\pi^4 a c^{2/3}\sqrt{-\eta_0 c^{-1/3}}\equiv\pm\gamma^{-1/3}\widetilde{M}(\widetilde{E}-\widetilde{E}_b)^{1/2}. \tag{3.33}$$

With the help of these relations the semiclassical oscillator strength (3.30) can be expressed in terms of the parameters $\widetilde{\sigma}$ and $\widetilde{M}$ that follow directly from the classical trajectory calculations. The final result for the contribution of a fold catastrophe thus reads

$$f^{\mathrm{osc}}=2(E-E_i)\sqrt{\sin\vartheta_i\sin\vartheta_f}\,\mathcal{Y}_m(\vartheta_i)\mathcal{Y}_m(\vartheta_f)2^{7/2}\times\pi^2\gamma^{1/9}(3\widetilde{\sigma}/2)^{1/6}|\widetilde{M}|^{-1/2}\times\mathrm{Ai}((3\widetilde{\sigma}/2)^{2/3}\gamma^{-2/9}(\widetilde{E}_b-\widetilde{E}))\times\sin\left(S_m^0-\frac{\pi}{2}\mu^0\right). \tag{3.34}$$

It is also illustrative to investigate the asymptotic behavior of Eqs. (3.30) and (3.34) in the limit $c\,\eta_0\gg 0$; i.e., at energies $\widetilde{E}$ below the bifurcation energy $\widetilde{E}_b$, where no orbit returns to the origin, because this reveals the role of the complex ''ghost'' orbits discussed in Sec. B 1. In the case $\widetilde{E}\ll\widetilde{E}_b$ the asymptotic form of the Airy function (see Appendix B 1) can be used in Eq. (3.34) to obtain

$$f^{\mathrm{osc}}=2(E-E_i)\sqrt{\sin\vartheta_i\sin\vartheta_f}\,\mathcal{Y}_m(\vartheta_i)\mathcal{Y}_m(\vartheta_f)2(2\pi)^{3/2}\times\gamma^{1/6}|\widetilde{M}|^{-1/2}(\widetilde{E}_b-\widetilde{E})^{-1/4}\times\mathrm{Im}\left\{\exp\left(i\left[S_m^0+i\widetilde{\sigma}\gamma^{-1/3}(\widetilde{E}_b-\widetilde{E})^{3/2}-\frac{\pi}{2}\mu^0\right]\right)\right\}. \tag{3.35}$$

Formally this equation coincides with Eq. (3.21), but for a closed orbit with a complex action and imaginary monodromy matrix element

$$S=S_m^0+i\,\gamma^{-1/3}\widetilde{\sigma}(\widetilde{E}_b-\widetilde{E})^{3/2}, \tag{3.36}$$

$$m_{12}=i\,\gamma^{-1/3}\widetilde{M}(\widetilde{E}_b-\widetilde{E})^{1/2}. \tag{3.37}$$

This is precisely the behavior found in the investigation of ghost orbits at energies below a saddle-node bifurcation (see Sec. II A). Obviously, as one moves away from the bifurcation point to smaller energies, the positive imaginary part of S grows, and thus the contribution of the ghost orbit to the semiclassical oscillator strength is damped exponentially.

In the classical calculations, the complex-conjugate ghost, with negative imaginary part of the action, also exists. In the above semiclassical formulas this complex-conjugate ghost would produce an unphysical exponential increase of the amplitude at energies below the bifurcation point. Thus we have as a by-product of the derivation of uniform semiclassical formulas that ghost orbits of this type have no physical meaning. In other words, they must not be included in the standard formula (3.21) since they do not appear in the asymptotic expansion of the uniform approximation of the oscillator strength.

The uniform solution (3.34) for the fold catastrophe has the benefit of connecting both asymptotic situations, the contribution of the physical ghost orbit at energies below the

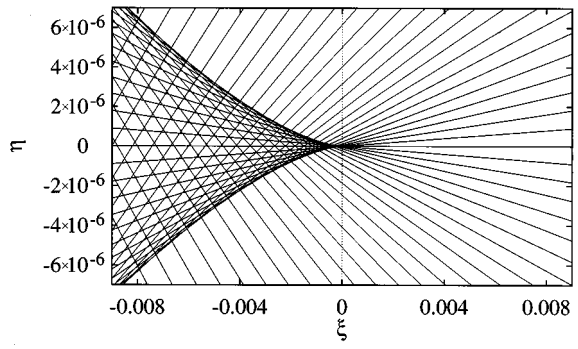

FIG. 7. Cusp catastrophe of returning orbits (in rotated semiparabolic coordinates) related to the period-doubling bifurcation of the balloon orbit V_1^1 at bifurcation energy $\widetilde{E}_b=-0.342\,025\,8$.

saddle-node bifurcation and the two real orbits at energies above the bifurcation, without exhibiting any singularity at the bifurcation point.

D. The cusp catastrophe

The second fundamental catastrophe is the cusp, as it occurs, for example, at the period-doubling bifurcation of the balloon orbit V_1^1 at scaled energy $\widetilde{E}_b=-0.342\,025\,8$ (see Sec. II B). The Hamilton-Jacobi equations for the returning orbits at the cusp read (with $p_\xi=\partial S/\partial\xi$ and $p_\eta=\partial S/\partial\eta$)

$$2cp_\eta^3+p_\xi^2[(\xi-\xi_0)p_\eta-\eta p_\xi]=0,$$
$$p_\xi^2+p_\eta^2=4, \tag{3.38}$$

and we obtain (with $p_\eta/p_\xi\approx a\Delta\vartheta_i$ and parameters a, c, and ξ_0 specified later)

$$\eta(\xi)=2a^3c(\Delta\vartheta_i)^3+a(\Delta\vartheta_i)(\xi-\xi_0). \tag{3.39}$$

The bunch of orbits forming the cusp is shown in Fig. 7. Equation (3.39) is a cubic polynomial in $\Delta\vartheta_i$ with one or three real zeros, depending on the sign of

$$D=27c\,\eta^2+2(\xi-\xi_0)^3. \tag{3.40}$$

Both regions are separated by a caustic given by $D=0$, i.e., $\eta^2=(2/27c)(\xi_0-\xi)^3$. In contrast to the fold catastrophe there is no classical forbidden region without any real solution of Eq. (3.39).

We shall now derive a uniform semiclassical approximation for the cusp catastrophe. The decisive point is again to find a solution for the classical action and the determinant in Eq. (3.11). Solving the Hamilton-Jacobi equations (3.38) in the vicinity of the central returning orbit ($r\gg0$, $\vartheta\approx\vartheta_f$) we obtain the classical action

$$\Delta S^\lambda(r,\vartheta)=\pm\sqrt{8r}+\tfrac{1}{4}\xi_0(\vartheta-\vartheta_f)^2-\tfrac{1}{16}c(\vartheta-\vartheta_f)^4 \tag{3.41}$$

and for the determinant in the denominator of Eq. (3.11) we have

$$\det\left(\frac{\partial(\mu,\nu)}{\partial(\tau,\vartheta_i)}\right)^\lambda=\det\left(\frac{\partial(\xi,\eta)}{\partial(\tau,\vartheta_i)}\right)^\lambda\underset{r\gg0}{\sim}\pm a\sqrt{8r},\quad \vartheta\approx\vartheta_f. \tag{3.42}$$

After summing up the contributions of the incoming and outgoing orbit (with the correct Maslov indices $\Delta\mu^{\rm out}=+2$, $\Delta\mu^{\rm in}=-1$), the stationary phase integral in Eq. (3.11) for the cusp catastrophe reads (with $t\equiv\vartheta-\vartheta_f$)

$$I(r)=2^{1/4}r^{-1/4}|a|^{-1/2}\exp\left(-i\frac{\pi}{4}\right)\cos\left(\sqrt{8r}-\frac{3}{4}\pi\right)\times\int_{-\infty}^{+\infty}\exp\{i[(\xi_0/4)t^2-(c/16)t^4]\}dt. \tag{3.43}$$

From Eq. (3.11) we now obtain the amplitude

$$\mathcal{A}=2^{5/2}\pi|a|^{-1/2}\exp\left(-i\frac{\pi}{4}\right)c^{-1/4}\Phi(-c^{-1/2}\xi_0), \tag{3.44}$$

where

$$\Phi(x)\equiv\int_{-\infty}^{+\infty}\exp(-i[xt^2+t^4])dt \tag{3.45}$$

is a special case of Pearcey's integral [25] that can be solved analytically (see Appendix B 2). Inserting the amplitude $\mathcal{A}$ [Eq. (3.44)] into Eq. (3.10) we finally obtain the contribution of the cusp to the total oscillator strength (3.1)

$$f^{\rm osc}=2(E-E_i)\sqrt{\sin\vartheta_i\sin\vartheta_f}\,\mathcal{Y}_m(\vartheta_i)\mathcal{Y}_m(\vartheta_f)2^{5/2}\pi\times|a|^{-1/2}c^{-1/4}{\rm Im}\left\{\exp\left(i\left[S_m^0-\frac{\pi}{2}\mu^0\right]\right)\Phi(-c^{-1/2}\xi_0)\right\}. \tag{3.46}$$

To find the relation between the parameters a, c, and ξ_0 and parameters of the closed classical orbits we proceed in an analogous manner as for the fold, and discuss the asymptotic behavior of Eq. (3.46) in the limit $\xi_0\ll0$ and $\xi_0\gg0$, i.e., at scaled energies far from the bifurcation point. Applying the asymptotic formulas for $\Phi(x)$ [Eq. (B9) of Appendix B 2] we obtain

$$f^{\rm osc}=2(E-E_i)\sqrt{\sin\vartheta_i\sin\vartheta_f}\,\mathcal{Y}_m(\vartheta_i)\mathcal{Y}_m(\vartheta_f)2(2\pi)^{3/2}|a\xi_0|^{-1/2}\times\begin{cases}\sin\left[S_m^0-\dfrac{\pi}{2}(\mu^0+1)+\dfrac{\pi}{4}\right]; & \xi_0\ll0\\ \sin\left(S_m^0-\dfrac{\pi}{2}\mu^0+\dfrac{\pi}{4}\right)+\sqrt{2}\sin\left[S_m^0+\dfrac{\xi_0^2}{4c}-\dfrac{\pi}{2}(\mu^0+1)+\dfrac{\pi}{4}\right]; & \xi_0\gg0.\end{cases} \tag{3.47}$$

By comparing with Eq. (3.21) and with the classical dynamics at the period-doubling bifurcation (see Sec. II B) we find the following physical interpretation of Eq. (3.47). There is one real closed orbit with classical action S_m^0 which exists both below and above the bifurcation point. The Maslov index of this orbit changes by one when the orbit undergoes the bifurcation and the monodromy matrix element m_{12} must obey the relation

$$m_{12} = -a\xi_0 \equiv -\gamma^{-1/3}\widetilde{M}(\widetilde{E}-\widetilde{E}_b). \tag{3.48}$$

The remaining term at $\xi_0 \gg 0$ can be interpreted as the sum of two real orbit contributions with the Maslov index μ^0+1 and classical action and monodromy matrix element

$$S = S_m^0 + \frac{1}{4c}\xi_0^2 \equiv S_m^0 + \gamma^{-1/3}\widetilde{\sigma}(\widetilde{E}-\widetilde{E}_b)^2, \tag{3.49}$$

$$m_{12} = 2a\xi_0 \equiv 2\gamma^{-1/3}\widetilde{M}(\widetilde{E}-\widetilde{E}_b). \tag{3.50}$$

In the investigation of closed orbits around the period-doubling bifurcation (Sec. II B), in addition to the real orbits, two ghost orbits have been found at energies below the bifurcation energy with the somewhat strange property that the classical action S and monodromy matrix element m_{12} both remain real, although the coordinates and momenta in phase space are complex. Contrary to the fold catastrophe, in the asymptotic expansion (3.47) of the uniform solution (3.46) for a cusp, no ghost contribution appears; i.e., these two ghost orbits are both without physical meaning in the photoabsorption process. With the help of Eqs. (3.49) and (3.50) we can finally express the uniform solution (3.46) completely in terms which are accessible from closed-orbit calculations

$$\begin{aligned} f^{\mathrm{osc}} = {} & 2(E-E_i)\sqrt{\sin\vartheta_i \sin\vartheta_f}\,\mathcal{Y}_m(\vartheta_i)\mathcal{Y}_m(\vartheta_f) 8\pi\gamma^{1/12}\widetilde{\sigma}^{1/4} \\ & \times |\widetilde{M}|^{-1/2}\,\mathrm{Im}\left\{ \exp\left(i\left[S_m^0 - \frac{\pi}{2}\mu^0 \right] \right) \right. \\ & \left. \times \Phi[2\widetilde{\sigma}^{1/2}\gamma^{-1/6}(\widetilde{E}_b-\widetilde{E})] \right\}. \end{aligned} \tag{3.51}$$

E. The butterfly catastrophe

As an example of even more complicated catastrophes we investigate in this section the bifurcation of R_2, i.e., the second return of the perpendicular orbit around the scaled energy $\widetilde{E} = -0.316$. A detailed classical analysis (see Sec. II C) exhibits a sequence of two different elementary types of bifurcations at almost the same point. At the scaled energy $\widetilde{E}_b^{(1)} = -0.317\,353\,45$ two closed orbits, namely, R_2^1 and a second orbit with similar shape, which we call R_2^{1b}, are created by a saddle-node bifurcation related to a fold catastrophe. At the only slightly higher energy $\widetilde{E}_b^{(2)} = -0.316\,185\,37$ the orbit R_2^{1b} already vanishes again in a period-doubling bifurcation with the second return of the perpendicular orbit R_2, i.e., in a catastrophe where neighboring returning orbits form a cusp. The energy spacing between both bifurcations is so small that they cannot be treated as isolated, and none of the uniform formulas Eq. (3.34) for the fold and Eq. (3.51) for the cusp, can be applied in a semiclassical calculation of oscillator strengths. The correct uniform approximation must describe both bifurcations simultaneously, i.e., a more complicated type of catastrophe, viz. a butterfly catastrophe, must be investigated.

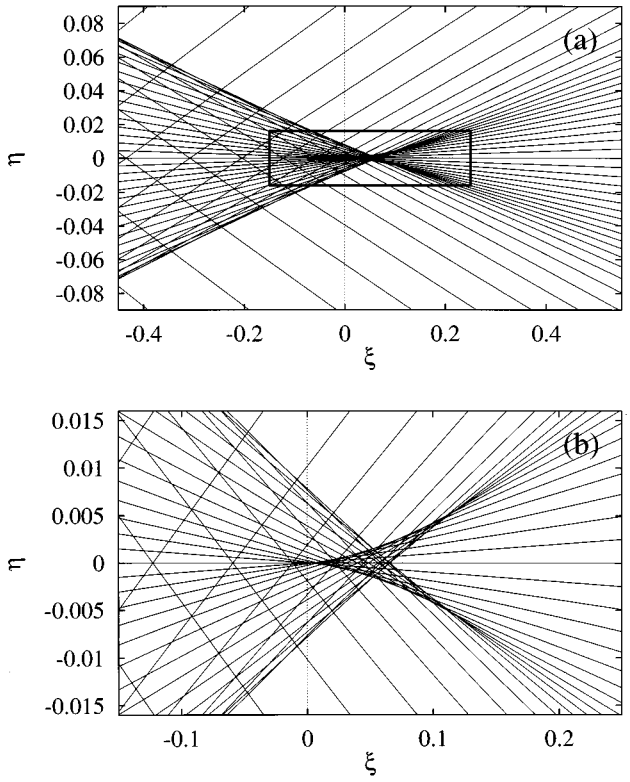

FIG. 8. (a) Butterfly catastrophe of returning orbits (in rotated semiparabolic coordinates) related to the bifurcation of the perpendicular orbit at $\widetilde{E}_b = -0.316\,185\,37$. (b) Magnification of the marked region close to the nucleus. There are one, three, or five orbits returning to each point (ξ, η) in phase space.

The bunch of trajectories forming the butterfly is given by the Hamilton-Jacobi equations (with $p_\xi = \partial S/\partial\xi$ and $p_\eta = \partial S/\partial\eta$)

$$\begin{aligned} & 3dp_\eta^5 + 2cp_\xi^2 p_\eta^3 + p_\xi^4[(\xi-\xi_0)p_\eta - \eta p_\xi] = 0, \\ & p_\xi^2 + p_\eta^2 = 4, \end{aligned} \tag{3.52}$$

where the parameters c, d, and ξ_0 will be specified later. With $p_\eta/p_\xi \approx a\Delta\vartheta_i$ we obtain

$$\eta(\xi) = 3a^5 d(\Delta\vartheta_i)^5 + 2a^3 c(\Delta\vartheta_i)^3 + a(\Delta\vartheta_i)(\xi-\xi_0). \tag{3.53}$$

The butterfly is illustrated in Fig. 8. Depending on the number of real solutions $\Delta\vartheta_i$ of Eq. (3.53) there exist one, three, or five orbits returning to each point (ξ, η). The different regions are separated by caustics.

To find a uniform semiclassical approximation for the butterfly catastrophe, we have to solve the Hamilton-Jacobi equations (3.52), at least in the vicinity of the central returning orbit, and to insert the action $S(r, \vartheta)$ into Eq. (3.11). For the classical action we obtain

$$\Delta S^{\lambda}(r,\vartheta)=\pm\sqrt{8r}+\tfrac{1}{4}\xi_0(\vartheta-\vartheta_f)^2+\tfrac{1}{16}c(\vartheta-\vartheta_f)^4 -\tfrac{1}{64}d(\vartheta-\vartheta_f)^6, \tag{3.54}$$

and for the determinant in the denominator of Eq. (3.11) we find $\pm a\sqrt{8r}$ in the limit $r\gg 0$ and $\vartheta\approx\vartheta_f$, i.e., the same result (3.42) as for the cusp. Summing up in Eq. (3.11) the contributions of the incoming and the outgoing orbit (with Maslov indices $\Delta\mu^{\lambda}$ as for the cusp) we obtain the integral $I(r)$ and the amplitude $\mathcal{A}$ for the butterfly catastrophe ($t\equiv\vartheta-\vartheta_f$)

$$I(r)=2^{1/4}r^{-1/4}|a|^{-1/2}\exp\left(-i\frac{\pi}{4}\right)\cos\left(\sqrt{8r}-\frac{3}{4}\pi\right) \times\int_{-\infty}^{+\infty}\exp\{i[(\xi_0/4)t^2-(c/16)t^4-(d/64)t^6]\}dt, \tag{3.55}$$

$$\Rightarrow\mathcal{A}=2^{5/2}\pi|a|^{-1/2}\exp\left(-i\frac{\pi}{4}\right)d^{-1/6}\Psi(-d^{-1/3}\xi_0,-cd^{-2/3}), \tag{3.56}$$

where

$$\Psi(x,y)\equiv\int_{-\infty}^{+\infty}\exp(-i[xt^2+yt^4+t^6])dt \tag{3.57}$$

is an analytic function in both variables x and y. Its numerical calculation and asymptotic properties are discussed in Appendix B 3. The uniform result for the oscillatory part of the transition strength now reads

$$f^{\mathrm{osc}}=2(E-E_i)\sqrt{\sin\vartheta_i\sin\vartheta_f}\,\mathcal{Y}_m(\vartheta_i)\mathcal{Y}_m(\vartheta_f)2^{5/2}\pi \times|a|^{-1/2}d^{-1/6} \times\mathrm{Im}\left\{\exp\left(i\left[S_m^0-\frac{\pi}{2}\mu^0\right]\right)\Psi(-d^{-1/3}\xi_0,-cd^{-2/3})\right\}. \tag{3.58}$$

It is very illustrative to study the asymptotic behavior of the uniform approximation (3.58) as we obtain, on the one hand, the relation between the parameters a, c, d, and ξ_0 and the actions and the monodromy matrix elements of closed classical orbits, and, on the other hand, the role of complex ghost orbits related to this type of bifurcation is revealed. In the following we discuss both limits $\xi_0\gg 0$, i.e., scaled energy $\widetilde{E}\gg\widetilde{E}_b^{(2)}$, and $\xi_0\ll 0$, i.e., $\widetilde{E}\ll\widetilde{E}_b^{(1)}$.

1. Asymptotic behavior at scaled energy $\widetilde{E}\gg\widetilde{E}_b^{(2)}$

Applying Eq. (B13) from Appendix B 3 to the Ψ function in the uniform approximation (3.58), we obtain the asymptotic formula for $\xi_0\gg 0$

$$f^{\mathrm{osc}}=2(E-E_i)\sqrt{\sin\vartheta_i\sin\vartheta_f}\,\mathcal{Y}_m(\vartheta_i)\mathcal{Y}_m(\vartheta_f)2(2\pi)^{3/2} \times|a\xi_0|^{-1/2}\Bigg\{\sin\left(S_m^0-\frac{\pi}{2}\mu^0+\frac{\pi}{4}\right) +\left[1+\frac{c^2}{3d\xi_0}[1+\sqrt{(3d/c^2)\xi_0+1}]\right]^{-1/2} \times\sin\left(S_m^0+\frac{c^3}{9d^2}\left\{\frac{3d}{c^2}\xi_0+\frac{2}{3}\left[1+\left(1+\frac{3d}{c^2}\xi_0\right)^{3/2}\right]\right\} -\frac{\pi}{2}(\mu^0+1)+\frac{\pi}{4}\right)\Bigg\}. \tag{3.59}$$

Comparing this with Eq. (3.21) we can identify the contributions of three real closed orbits. The classical action of orbit 1 is S_m^0, its Maslov index is μ^0 and the monodromy matrix element m_{12} is given by

$$m_{12}^{(1)}=-a\xi_0\equiv-\gamma^{-1/3}\widetilde{M}(\widetilde{E}-\widetilde{E}_b), \tag{3.60}$$

where the parameter $\widetilde{M}$ can be determined by closed-orbit calculations (see Sec. II C). Orbits 2 and 3 are symmetric with respect to the $z=0$ plane and have the same orbital parameters, i.e., Maslov index μ^0+1 and the classical action and the monodromy matrix element

$$S^{(2,3)}=S_m^0+\Delta S =S_m^0+\frac{c^3}{9d^2}\left\{\frac{3d}{c^2}\xi_0+\frac{2}{3}\left[1+\left(\frac{3d}{c^2}\xi_0+1\right)^{3/2}\right]\right\}, \tag{3.61}$$

$$m_{12}^{(2,3)}=4a\xi_0\left[1+\frac{c^2}{3d\xi_0}[1+\sqrt{(3d/c^2)\xi_0+1}]\right]. \tag{3.62}$$

In the example of the bifurcation of orbit R_2 at scaled energy $\widetilde{E}_b^{(2)}=-0.316\,185\,37$, orbit 1 is the orbit R_2 perpendicular to the magnetic-field axis, while orbits 2 and 3 can be identified with R_2^1 traversed in both directions ($\vartheta_{i,3}=\pi-\vartheta_{i,2}$). With the help of Eqs. (3.60) to (3.62) and classical scaling properties of the action and the monodromy matrix the parameters a, c, d, and ξ_0 in the uniform approximation (3.58) can now be expressed completely in terms of closed-orbit parameters k, $\widetilde{\sigma}$, and $\widetilde{M}$ (see Sec. II C),

$$|a|^{-1/2}d^{-1/6}=3^{1/6}\gamma^{1/18}k^{1/3}(\widetilde{\sigma}/\widetilde{M})^{1/2},$$
$$d^{-1/3}\xi_0=3^{1/3}k^{2/3}\gamma^{-2/9}\widetilde{\sigma}(\widetilde{E}-\widetilde{E}_b^{(2)}),$$
$$cd^{-2/3}=(9k)^{1/3}\gamma^{-1/9}. \tag{3.63}$$

In the classical analysis complex ghost orbits were discovered both below and above the bifurcation energy. At $\widetilde{E}>\widetilde{E}_b^{(2)}$ they have the property that the classical action and the monodromy matrix remain real, although coordinates and momenta in phase space are complex. These ghost orbits do not appear in the asymptotic expansion (3.59) of the uniform approximation (3.58), and therefore, in analogy with the cusp catastrophe, they do not have a physical meaning. The situ-

ation is different at energy $\widetilde{E}<\widetilde{E}_b^{(1)}$ where a ''hidden ghost'' with physical meaning will be revealed in Sec. III E 2.

2. Asymptotic behavior and ''hidden ghost'' at scaled energy $\widetilde{E}\ll\widetilde{E}_b^{(1)}$

At scaled energies below the bifurcation point we can apply the asymptotic formula (B15) from Appendix B 3 to the Ψ function in the uniform approximation (3.58) and obtain

$$\begin{aligned} f^{\rm osc}=&2(E-E_i)\sqrt{\sin\vartheta_i\sin\vartheta_f}\,\mathcal{Y}_m(\vartheta_i)\mathcal{Y}_m(\vartheta_f)2(2\pi)^{3/2}\\ &\times|a\xi_0|^{-1/2}\Bigg\{\sin\Bigg(S_m^0-\frac{\pi}{2}(\mu^0+1)+\frac{\pi}{4}\Bigg)\\ &+\mathrm{Im}\Bigg\{\Bigg[1+\frac{c^2}{3d\xi_0}[1-i\sqrt{-(3d/c^2)\xi_0-1}]\Bigg]^{-1/2}\\ &\times\exp\Bigg(i\Bigg[S_m^0+\frac{c^3}{9d^2}\Bigg\{\frac{3d}{c^2}\xi_0\\ &+\frac{2}{3}\Bigg[1+i\Bigg(-\frac{3d}{c^2}\xi_0-1\Bigg)^{3/2}\Bigg]\Bigg\}-\frac{\pi}{2}\mu^0+\frac{\pi}{4}\Bigg]\Bigg)\Bigg\}\Bigg\}. \end{aligned} \tag{3.64}$$

The first term in Eq. (3.64) can be identified as a real orbit with the same classical action and monodromy matrix element as in Eq. (3.59), but with a Maslov index increased by one. The second term in Eq. (3.64) is a ghost orbit contribution resulting from a superposition of two closed orbits with complex action and monodromy matrix element,

$$S^{(2,3)}=S_m^0+\frac{c^3}{9d^2}\Bigg\{\frac{3d}{c^2}\xi_0+\frac{2}{3}\Bigg[1+i\Bigg(-\frac{3d}{c^2}\xi_0-1\Bigg)^{3/2}\Bigg]\Bigg\}, \tag{3.65}$$

$$m_{12}^{(2,3)}=4a\xi_0\Bigg[1+\frac{c^2}{3d\xi_0}[1-i\sqrt{-(3d/c^2)\xi_0-1}]\Bigg], \tag{3.66}$$

traversed in both directions. The positive imaginary part of the classical action results in an exponential damping of the ghost orbit contribution to the oscillator strength amplitude with decreasing energy similar to the situation at a fold catastrophe discussed above. In contrast to the fold, however, the ghost orbit related to a butterfly catastrophe is always accompanied by a real orbit with almost the same classical action. Because the contribution of the real orbit is not exponentially damped its amplitude at energies where the asymptotic formula (3.64) is valid is much stronger than the ghost contribution. Therefore we call the ghost orbit in Eq. (3.64) a ''hidden ghost,'' and it might be rather difficult to find evidence for such a hidden ghost orbit related to a butterfly catastrophe in the Fourier transform of, e.g., experimental scaled energy spectra.

Note that, classically, the complex conjugate of the hidden ghost orbit also exists. The negative imaginary part of its classical action would result in an unphysical exponential increase of amplitude with decreasing energy, and consequently the complex-conjugate ghost orbit does not appear in the asymptotic formula (3.64).

Finally, after inserting Eq. (3.63) in Eq. (3.58), the uniform approximation for the butterfly catastrophe reads

$$\begin{aligned} f^{\rm osc}=&2(E-E_i)\sqrt{\sin\vartheta_i\sin\vartheta_f}\,\mathcal{Y}_m(\vartheta_i)\mathcal{Y}_m(\vartheta_f)\\ &\times\pi\gamma^{1/18}3^{1/6}k^{1/3}(32\widetilde{\sigma}/\widetilde{M})^{1/2}\\ &\times\mathrm{Im}\Bigg\{\exp\Bigg(i\Bigg[S_m^0-\frac{\pi}{2}\mu^0\Bigg]\Bigg)\\ &\times\Psi(-3^{1/3}k^{2/3}\gamma^{-2/9}\widetilde{\sigma}(\widetilde{E}-\widetilde{E}_b^{(2)}),-(9k)^{1/3}\gamma^{-1/9})\Bigg\}. \end{aligned} \tag{3.67}$$

IV. RESULTS AND DISCUSSION

We now discuss the effects of bifurcations and ghost orbits on photoabsorption spectra of the hydrogen atom in a magnetic field and compare the uniform semiclassical results derived in the preceding chapter to solutions of standard closed-orbit theory. Semiclassically each closed orbit generates a modulation in the photoabsorption cross section. Here we are not interested in the energy and field dependence of these modulations, which are directly related to the classical action S of closed orbits, but in the behavior of their *amplitudes*, especially in the vicinity of bifurcations. In the following we also drop the common prefactor:

$$2(E-E_i)(\sin\vartheta_i\sin\vartheta_f)^{1/2}\mathcal{Y}_m(\vartheta_i)\mathcal{Y}_m(\vartheta_f)$$

in formulas for the oscillatory part $f^{\rm osc}$ of the photoabsorption cross section. This prefactor depends on the inital state and excitation process (see Appendix A) and is, for low-lying initial states, a slowly varying function of the initial and final angles of closed orbits. The amplitude $A(\widetilde{E},\gamma)$ can now be defined as

$$A(\widetilde{E},\gamma)=\Bigg|\sum_k\mathcal{A}_k(\widetilde{E},\gamma)\exp\Bigg(i\Bigg[S_m^k(\widetilde{E},\gamma)-\frac{\pi}{2}\mu^k+\frac{\pi}{4}\Bigg]\Bigg)\Bigg|. \tag{4.1}$$

By taking the absolute value instead of the imaginary part in Eq. (4.1) we suppress, for the graphical presentation of results, the high oscillatory modulations caused by the energy and field dependence of the classical action $S_m^k(\widetilde{E},\gamma)$. Nevertheless, the exponential function in Eq. (4.1) is important when applying Eq. (4.1) to nonuniform standard solutions of closed-orbit theory with coefficients $\mathcal{A}_k$ given by Eq. (3.20), i.e., (in scaled variables)

$$\mathcal{A}_k=2(2\pi)^{3/2}\gamma^{1/6}[\widetilde{m}_{12,k}(\widetilde{E})]^{-1/2}. \tag{4.2}$$

In this case we add, in Eq. (4.1), the contributions of all real closed orbits and ghosts k which are included in the corresponding uniform approximation. Interference effects between these orbits are now taken care of by the exponential function. Furthermore, the classical action of ghost orbits may be complex, which results, for a positive imaginary part of the action, in an exponential damping of ghost orbit contributions. Note that the energy dependence of amplitudes (4.1) can be measured experimentally by *scaled energy spec-*

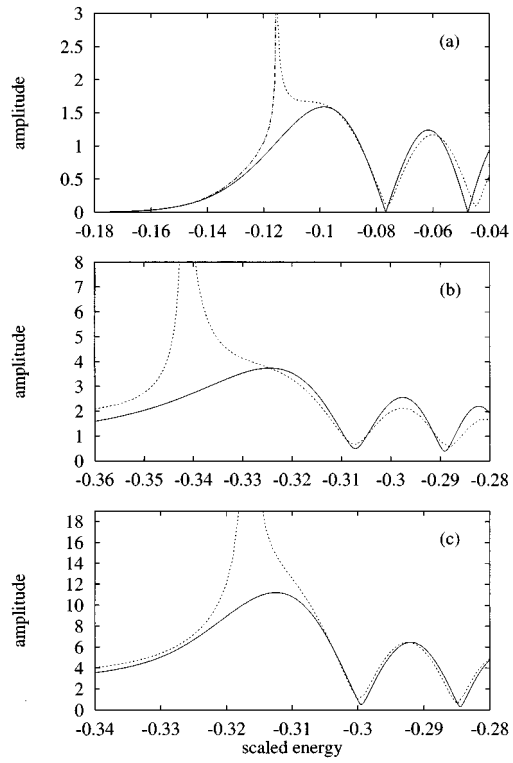

FIG. 9. Semiclassical amplitudes. (a) X_1 (fold catastrophe), magnetic field strength $\gamma=4\times10^{-6}$ a.u.; (b) V_2^2 (cusp catastrophe), $\gamma=10^{-7}$; (c) R_2 (butterfly catastrophe), $\gamma=10^{-7}$. Dashed lines: Amplitudes in the standard model. Dashed-dotted line [in (a)]: Ghost orbit contribution. Solid lines: Uniform approximations.

troscopy [3,9,21] when following the peak hights of resonances in the $(\widetilde{E},\widetilde{S})$ diagram of Fourier transform action spectra.

First we discuss the fold catastrophe related to the saddle-node bifurcation of orbit X_1. The amplitudes $A(\widetilde{E},\gamma)$ at constant magnetic-field strength $\gamma=4\times10^{-6}$ are presented in Fig. 9(a). The dashed line shows the superposition of the two real orbits X_1^a and X_1^b at energies $\widetilde{E}>\widetilde{E}_b$. The oscillatory structure of the amplitude is the result of a strong interference between these two orbits. At the bifurcation energy the amplitude diverges. Note that the amplitude at energies below the bifurcation point is zero in the standard formulation of the closed-orbit theory, i.e., when only real orbits are considered. The dashed-dotted line is the extension when ghost orbit contributions are also included. We only consider the ghost with a positive imaginary part of complex action because only this ghost has a physical meaning (see the discussion in Sec. III C). The amplitude decreases exponentially in $-(\widetilde{E}_b-\widetilde{E})^{3/2}$ with decreasing energy, but also exhibits an unphysical divergence at the bifurcation point. The solid line in Fig. 9(a) is the uniform approximation for the amplitude which we obtain from Eq. (3.34) as

$$A(\widetilde{E},\gamma)=2^{7/2}\pi^2\gamma^{1/9}(3\widetilde{\sigma}/2)^{1/6}|\widetilde{M}|^{-1/2}\times|\mathrm{Ai}((3\widetilde{\sigma}/2)^{2/3}\gamma^{-2/9}(\widetilde{E}_b-\widetilde{E}))|, \tag{4.3}$$

with parameters $\widetilde{E}_b$, $\widetilde{\sigma}$, and $\widetilde{M}$ determined from the classical trajectory calculations in Sec. II A. Apart from constant factors, the uniform approximation to the amplitude is an Airy function in terms of the energy difference $\widetilde{E}_b-\widetilde{E}$. Both the oscillatory structure of the amplitude at $\widetilde{E}>\widetilde{E}_b$ and the exponentially damped ghost orbit tail are well reproduced, but, in addition, the singularity at the bifurcation point is now completely removed. Note that the maximum of the amplitude is not located at the bifurcation point $\widetilde{E}=\widetilde{E}_b$ but is shifted to a slightly higher energy.

The results for the cusp catastrophe related to the period-doubling bifurcation of the balloon orbit V_1^1 are illustrated in Fig. 9(b) (magnetic-field strength $\gamma=10^{-7}$). The nonuniform amplitude is plotted as a dashed line. Above the bifurcation energy, three real orbits, the period-doubled balloon, V_2^2, and the bifurcated orbit, V_2^{2*}, traversed in both directions, are considered in Eq. (4.1), and the interference of these three orbits produces the oscillatory fluctuations of the amplitude. As discussed in Sec. III D the ghost orbits related to the cusp catastrophe have no physical meaning and, therefore, only the real orbit, i.e., the period doubled balloon V_2^2, is considered at $\widetilde{E}<\widetilde{E}_b$. The nonuniform solution is characterized by an unphysical divergence of the amplitude around the bifurcation energy, but the singularity is removed in the uniform approximation [solid line in Fig. 9(b)]

$$A(\widetilde{E},\gamma)=8\pi\gamma^{1/12}\widetilde{\sigma}^{1/4}|\widetilde{M}|^{-1/2}|\Phi(2\widetilde{\sigma}^{1/2}\gamma^{-1/6}(\widetilde{E}_b-\widetilde{E}))| \tag{4.4}$$

obtained from Eq. (3.51), and with the classical parameters $\widetilde{E}_b$, $\widetilde{\sigma}$, and $\widetilde{M}$ determined in Sec. II B. The energy dependence is given by a special case of Pearcey's integral, $\Phi(x)$ (see Appendix B 2). In contrast to the fold catastrophe [Fig. 9(a)] there is a real orbit, instead of a ghost orbit, below the bifurcation point and therefore the amplitude decreases $\sim(\widetilde{E}_b-\widetilde{E})^{-1/2}$ rather than exponentially with decreasing energy. The modulations of amplitudes at $\widetilde{E}>\widetilde{E}_b$ are also less pronounced, and, in particular, there are no energies with vanishing amplitude, i.e., with complete destructive interference between all closed-orbit contributions. Oscillations in periodic orbit contributions related to a cusp catastrophe of returning trajectories have recently been verified experimentally in Stark spectra of lithium atoms [21].

Finally we discuss the amplitudes of modulations for the butterfly catastrophe of returning trajectories. The butterfly catastrophe is related to a more complicated bifurcation scenario as found, e.g., around the period doubling of the perpendicular orbit (see Sec. II C). The uniform approximation to the amplitudes is obtained from Eq. (3.67),

$$A(\widetilde{E},\gamma)=\pi\gamma^{1/18}3^{1/6}k^{1/3}(32\widetilde{\sigma}/\widetilde{M})^{1/2}\times|\Psi[-3^{1/3}k^{2/3}\gamma^{-2/9}\widetilde{\sigma}(\widetilde{E}-\widetilde{E}_b^{(2)}),-(9k)^{1/3}\gamma^{-1/9}]|, \tag{4.5}$$

with the closed-orbit parameters k, $\widetilde{\sigma}$, $\widetilde{M}$, and $\widetilde{E}_b^{(2)}$ determined in Sec. II C and the integral $\Psi(x,y)$ solved in Appendix B 3. Results for $\gamma=10^{-7}$ are presented in Fig. 9(c). The solid line is the uniform approximation (4.5), and for comparison the dashed line shows the nonuniform solution of the standard closed-orbit theory. The modulations of amplitudes at energies above the bifurcation point are caused by the

interference of three closed orbits, namely, the period-doubled perpendicular orbit, R_2, and the ''Pacman'' orbit, R_2^1, traversed in both directions. Ghost orbits exist at these energies but have no physical meaning (see Sec. III E). Below the bifurcation point one real orbit, R_2, and, in addition, a ghost orbit (and its time reversed counterpart) contribute to the semiclassical photoabsorption spectrum. As in the case of a fold catastrophe the amplitude of the ghost orbit is damped exponentially with decreasing energy, but now the ghost is not isolated and its contribution is surpassed by that of the perpendicular orbit, i.e., the ghost is ''hidden'' behind the real orbit.

V. CONCLUSIONS

Photoabsorption spectra of hydrogen in a magnetic field, calculated semiclassically by application of closed-orbit theory in its original version [7,8], suffer from singularities at energies where orbits undergo bifurcations. The uniform approximations derived in this paper significantly improve on those calculations and remove unphysical singularities from the spectra. The total oscillator strength (3.1) is divided into three parts,

$$f = f^0 + \sum_{k_{\text{standard}}} f^{\text{osc}}_{k_{\text{standard}}} + \sum_{k_{\text{uniform}}} f^{\text{osc}}_{k_{\text{uniform}}}, \tag{5.1}$$

with f^0 the smoothly varying continous background and $f^{\text{osc}}_{k,\text{standard}}$ the oscillatory part from the contributions of isolated closed orbits sufficiently far away from any bifurcations. In this case the returning trajectories do not form a catastrophe at the origin and Eq. (3.21) can be applied. The third term in Eq. (5.1) adds the contributions of closed orbits near bifurcations, i.e., when returning trajectories form a catastrophe at the origin. The uniform approximations depend on the specific type of the catastrophe. In this paper we have investigated, in detail, the fold, cusp, and butterfly catastrophe, where $f^{\text{osc}}_{k,\text{uniform}}$ is given by Eqs. (3.34), (3.51), and (3.58), respectively. Note that each of these terms usually represents the contributions of several strongly interacting closed orbits including ghosts.

We believe that a large variety of singularities in semiclassical photoabsorption spectra of the hydrogen atom in a magnetic field can be removed by one of the uniform formulas mentioned above. The ''exotic'' orbits [3,9] are usually created in a saddle-node bifurcation, with the trajectories forming a fold close to the origin. As an example we have studied the shortest exotic orbit X_1, but obviously the uniform result for the fold catastrophe can be applied in all analogous situations. Also the uniform solution for the cusp catastrophe is not at all restricted to a period-doubling bifurcation of orbits (e.g., the period doubling of the balloon orbit V_1^1) but is valid for any period-n bifurcation whenever returning orbits form a cusp. Last, but not least, the perpendicular orbit R_1 undergoes an organized sequence of period-n bifurcations at energies $\widetilde{E} < -0.1273$, at which energy the orbit finally becomes unstable. The systematics of this sequence is explained in [11] by application of the normal form theory. The creation and annihilation of orbits R_μ^ν is similar to the bifurcation scenario of orbits R_2 and R_2^1 discussed in this paper, the returning orbits form a butterfly close to the origin, and the corresponding uniform approximations can be applied to semiclassical calculations of the photoabsorption cross section.

However, the set of catastrophes discussed in this paper is certainly not complete. The possible geometries of elementary catastrophes are systematically studied in catastrophe theory (see, e.g., [16]). A complete investigation of all types of catastrophes existing in atoms in external fields and the derivation of related uniform semiclassical approximations is subject to future work. For example, closed-orbit bifurcations might exist where the returning trajectories form a swallowtail. We also do not study bifurcations of the parallel orbit in this paper. The parallel orbit requires special treatment because of a symmetry property of nearby orbits which are invariant under rotations of the azimuthal angle, φ.

The application of uniform semiclassical approximations must not be restricted to the hydrogen atom. Investigations of nonhydrogenic atoms have revealed the importance of classical trajectories scattered at the ionic core [24]. The core scattering results in a dramatic increase in the number of closed orbit bifurcations which are related to singularities in the semiclassical photoabsorption spectra. Thus we expect uniform approximations to be a powerful tool to remove unphysical singularities from semiclassical spectra, not only of hydrogen but of nonhydrogenic atoms as well.

ACKNOWLEDGMENTS

We thank Professor F. Haake for stimulating discussions and for bringing ghost orbits to our attention. This work was supported by the Deutsche Forschungsgemeinschaft (SFB 237). J.M. is grateful to Alexander von Humboldt-Stiftung for financial assistance, and to Professor Howard Taylor for his kind hospitality at USC, where this work was completed.

APPENDIX A: ANGULAR FUNCTION $\mathcal{Y}_m(\vartheta)$

The angular function $\mathcal{Y}_m(\vartheta)$ solely depends on the initial state ψ_i and the dipole operator D and is a linear superposition of spherical harmonics

$$\mathcal{Y}_m(\vartheta) = \sum_{\ell=|m|}^{\infty} (-1)^\ell \mathcal{B}_{\ell m} Y_{\ell m}(\vartheta, 0). \tag{A1}$$

The coefficients $\mathcal{B}_{\ell m}$ are defined by the overlap integrals

$$\mathcal{B}_{\ell m} = \int d^3x (D\psi_i)(\mathbf{x}) \sqrt{2/r} J_{2\ell+1}(\sqrt{8r}) Y^*_{\ell m}(\vartheta, \varphi) \tag{A2}$$

[with $J_\nu(x)$ Bessel functions] and can be calculated analytically [8]. For excitations of the ground state $\psi_i = |1s0\rangle$ with π-polarized light (i.e., dipole operator $D = z$) the explicit result is

$$\mathcal{Y}_0(\vartheta) = -\pi^{-1/2} 2^3 e^{-2} \cos\vartheta \tag{A3}$$

and for $\psi_i = |2p0\rangle$; i.e., the initial state in many spectroscopic measurements on hydrogen [2,3,9] we obtain

$$\mathcal{Y}_0(\vartheta) = (2\pi)^{-1/2} 2^7 e^{-4} (4\cos^2\vartheta - 1). \tag{A4}$$

APPENDIX B: UNIFORM PHASE INTEGRALS

1. The Airy function Ai(x)

In the case of a fold catastrophe the uniform phase integral is an Airy function [26]

$$\int_{-\infty}^{+\infty}\cos(t^3+xt)dt=3^{-1/3}2\pi\mathrm{Ai}(3^{-1/3}x) \tag{B1}$$

with the asymptotic behavior

$$\mathrm{Ai}(\pm x)\underset{x\to\infty}{\sim}\begin{cases}\dfrac{1}{2}\pi^{-1/2}x^{-1/4}\exp\left(-\dfrac{2}{3}x^{3/2}\right)\\ \pi^{-1/2}x^{-1/4}\sin\left(\dfrac{2}{3}x^{3/2}+\dfrac{\pi}{4}\right)\end{cases}. \tag{B2}$$

2. The function $\Phi(x)$

For a cusp catastrophe the uniform phase integral

$$\Phi(x)\equiv\int_{-\infty}^{+\infty}\exp[-i(xt^2+t^4)]dt \tag{B3}$$

is a special case of Pearcey's integral [25,17,18]

$$P(x,y)=\int_{-\infty}^{+\infty}\exp[i(t^4+xt^2+yt)]dt, \tag{B4}$$

i.e.,

$$\Phi(x)=P^*(x,y=0). \tag{B5}$$

With the help of the integrals ($p>q>0$) [27]

$$\begin{aligned}\int_0^{\infty}&\exp[-i(x^p+tx^q)]dx\\ &=\frac{1}{p}\exp\left[-i\frac{\pi}{2p}\right]\sum_{k=0}^{\infty}\frac{1}{k!}\Gamma\left(\frac{kq+1}{p}\right)\\ &\quad\times\left(-t\exp\left[i\frac{p-q}{2p}\pi\right]\right)^k\end{aligned} \tag{B6}$$

we obtain an absolutely convergent Taylor series for $\Phi(x)$

$$\Phi(x)=\frac{1}{2}\exp\left[-i\frac{\pi}{8}\right]\sum_{n=0}^{\infty}\frac{1}{n!}\Gamma\left(\frac{2n+1}{4}\right)\left(x\exp\left[-i\frac{3}{4}\pi\right]\right)^n. \tag{B7}$$

Alternatively $\Phi(x)$ can be expressed in closed form in terms of Bessel functions [27]

$$\begin{aligned}\Phi(\pm x)=&\frac{\pi}{2}\sqrt{x/2}\exp\left[i\frac{x^2}{8}\right]\\ &\times\left\{\exp\left[-i\frac{\pi}{8}\right]J_{-1/4}\left(\frac{x^2}{8}\right)\mp\exp\left[i\frac{\pi}{8}\right]J_{1/4}\left(\frac{x^2}{8}\right)\right\}.\end{aligned} \tag{B8}$$

For large x we obtain asymptotic formulas by expanding the phases around their stationary points or by applying the asymptotic formula

$$J_\nu(x)\underset{x\to\infty}{\sim}\sqrt{(2/\pi x)}\cos\left(x-\frac{\pi\nu}{2}-\frac{\pi}{4}\right) \tag{B8}$$

of the Bessel functions to Eq. (B8)

$$\Phi(\pm x)\underset{x\to\infty}{\sim}\begin{cases}\sqrt{\pi/x}\exp\left[-i\dfrac{\pi}{4}\right]\\ \sqrt{\pi/x}\left\{\exp\left[i\dfrac{\pi}{4}\right]+\sqrt{2}\exp\left[i\left(\dfrac{1}{4}x^2-\dfrac{\pi}{4}\right)\right]\right\}\end{cases}. \tag{B9}$$

3. The function $\Psi(x,y)$

The uniform phase integral $\Psi(x,y)$ of the butterfly catastrophe is expanded in a two-parametric Taylor series around $x=y=0$

$$\begin{aligned}\Psi(x,y)&\equiv\int_{-\infty}^{+\infty}\exp[-i(xt^2+yt^4+t^6)]dt\\ &=\sum_{n=0}^{\infty}\sum_{m=0}^{\infty}\frac{1}{i^{n+m}}\frac{x^n y^m}{n!m!}\int_{-\infty}^{+\infty}t^{2n+4m}\exp[-it^6]dt.\end{aligned} \tag{B10}$$

With the substitution $z=t^{2n+4m+1}$ we obtain [27]

$$\begin{aligned}\int_{-\infty}^{+\infty}&t^{2n+4m}\exp[-it^6]dt\\ &=\frac{2}{2n+4m+1}\int_0^{\infty}\exp[-iz^{6/(2n+4m+1)}]dz\\ &=\frac{1}{3}\exp\left[-i\frac{2n+4m+1}{12}\pi\right]\Gamma\left(\frac{2n+4m+1}{6}\right),\end{aligned}$$

and finally

$$\begin{aligned}\Psi(x,y)=&\frac{1}{3}\exp\left[-i\frac{\pi}{12}\right]\sum_{n=0}^{\infty}\sum_{m=0}^{\infty}\frac{1}{n!m!}\Gamma\left(\frac{2n+4m+1}{6}\right)\\ &\times\left(x\exp\left[-i\frac{2}{3}\pi\right]\right)^n\left(y\exp\left[-i\frac{5}{6}\pi\right]\right)^m,\end{aligned} \tag{B11}$$

which is a convergent series for all x and y.

The asymptotic behavior of $\Psi(x,y)$ for $x\to\pm\infty$ is obtained in a stationary phase approximation to Eq. (B10), with the stationary points t_0 being defined by

$$t_0(6t_0^4+4yt_0^2+2x)=0. \tag{B12}$$

(a) $x\to-\infty$: There are three real stationary points given by

$$t_0=0\quad\text{and}\quad t_0^2=-\frac{1}{3}y+\left(\frac{1}{9}y^2-\frac{1}{3}x\right)^{1/2},$$

and we obtain

$$\Psi(x,y) \underset{x\to-\infty}{\sim} \int_{-\infty}^{+\infty} \exp[-ixt^2]dt + 2\exp[-i(xt_0^2+yt_0^4+t_0^6)] \times \int_{-\infty}^{+\infty} \exp[-i(x+6yt_0^2+15t_0^4)t^2]dt = \left(\frac{\pi}{-x}\right)^{1/2} \exp\left[i\frac{\pi}{4}\right] + \left[\frac{\pi}{-x+\frac{1}{3}y^2-y\left(\frac{1}{9}y^2-\frac{1}{3}x\right)^{1/2}}\right]^{1/2} \times \exp\left\{i\left[2\left(\frac{1}{9}y^2-\frac{1}{3}x\right)^{3/2}-\frac{1}{3}y\left(\frac{2}{9}y^2-x\right)-\frac{\pi}{4}\right]\right\}. \tag{B13}$$

(b) $x\to+\infty$: The only real solution of Eq. (B12) is $t_0=0$ and $\Psi(x,y)$ is approximated as

$$\Psi(x,y) \underset{x\to+\infty}{\sim} \int_{-\infty}^{+\infty} \exp[-ixt^2]dt = \left(\frac{\pi}{x}\right)^{1/2} \exp\left[-i\frac{\pi}{4}\right]. \tag{B14}$$

In the case of $y<0$ and $x\gtrsim\frac{1}{3}y^2$ the complex zeros

$$t_0=\pm\left[-\frac{1}{3}y\pm i(\tfrac{1}{3}x-\tfrac{1}{9}y^2)^{1/2}\right]^{1/2}$$

of Eq. (B12) are situated close to the real axis. When one considers these complex zeros in a stationary phase approximation Eq. (B14) is modified by an additional term exponentially damped for large x

$$\Psi(x,y) \underset{x\to+\infty}{\sim} \left(\frac{\pi}{x}\right)^{1/2} \exp\left[-i\frac{\pi}{4}\right] + \left[\frac{\pi}{x-\frac{1}{3}y^2-iy(\frac{1}{3}x-\frac{1}{9}y^2)^{1/2}}\right]^{1/2} \times \exp\left[-2\left(\frac{1}{3}x-\frac{1}{9}y^2\right)^{3/2}\right] \times \exp\left\{-i\left[\frac{1}{3}y\left(\frac{2}{9}y^2-x\right)-\frac{\pi}{4}\right]\right\}. \tag{B15}$$

[1] W. R. S. Garton and F. S. Tomkins, Astrophys. J. **158**, 839 (1969).

[2] A. Holle, G. Wiebusch, J. Main, B. Hager, H. Rottke, and K. H. Welge, Phys. Rev. Lett. **56**, 2594 (1986); J. Main, G. Wiebusch, A. Holle, and K. H. Welge, *ibid.* **57**, 2789 (1986).

[3] A. Holle, J. Main, G. Wiebusch, H. Rottke, and K. H. Welge, Phys. Rev. Lett. **61**, 161 (1988); J. Main, G. Wiebusch, and K. H. Welge, Comments At. Mol. Phys. **25**, 233 (1991).

[4] H. Friedrich and D. Wintgen, Phys. Rep. **183**, 37 (1989).

[5] H. Hasegawa, M. Robnik, and G. Wunner, Prog. Theor. Phys. Suppl. **98**, 198 (1989).

[6] S. Watanabe, in *Review of Fundamental Processes and Applications of Atoms and Ions*, edited by C. D. Lin (World Scientific, Singapore, 1993).

[7] M. L. Du and J. B. Delos, Phys. Rev. A **38**, 1896 (1988); **38**, 1913 (1988).

[8] E. B. Bogomolny, Pis'ma Zh. Éksp. Teor. Fiz. **47**, 445 (1988) [JETP Lett. **47**, 526 (1988)]; Zh. Éksp. Teor. Fiz. **96**, 487 (1989) [Sov. Phys. JETP **69**, 275 (1989)].

[9] J. Main, G. Wiebusch, K. H. Welge, J. Shaw, and J. B. Delos, Phys. Rev. A **49**, 847 (1994).

[10] J. M. Mao and J. B. Delos, Phys. Rev. A **45**, 1746 (1992).

[11] D. A. Sadovskiĭ, J. A. Show, and J. B. Delos, Phys. Rev. Lett. **75**, 2120 (1995); D. A. Sadovskiĭ and J. B. Delos, Phys. Rev. E **54**, 2033 (1996).

[12] M. V. Berry and K. E. Mount, Rep. Prog. Phys. **35**, 315 (1972).

[13] J. N. L. Connor, Mol. Phys. **31**, 33 (1976).

[14] M. V. Berry and C. Upstill, in *Progress in Optics*, edited by E. Wolf (North-Holland, Amsterdam, 1980), Vol. 18, p. 257–346.

[15] A. M. Ozorio de Almeida and J. H. Hannay, J. Phys. A **20**, 5873 (1987).

[16] T. Poston and I. N. Steward, *Catastrophe Theory and its Applications* (Pitman, London, 1978).

[17] J. N. L. Connor, Mol. Phys. **26**, 1217 (1973).

[18] J. N. L. Connor and D. Farrelly, J. Chem. Phys. **75**, 2831 (1981).

[19] A. D. Peters, C. Jaffé, and J. B. Delos, Phys. Rev. Lett. **73**, 2825 (1994).

[20] M. W. Beims and G. Alber, Phys. Rev. A **48**, 3123 (1993).

[21] M. Courtney, Hong Jiao, N. Spellmeyer, D. Kleppner, J. Gao, and J. B. Delos, Phys. Rev. Lett. **74**, 1538 (1995).

[22] M. Kuś, F. Haake, and D. Delande, Phys. Rev. Lett. **71**, 2167 (1993).

[23] E. L. Stiefel and G. Scheifele, *Linear and Regular Celestial Mechanics* (Springer, New York, 1971).

[24] B. Hüpper, J. Main, and G. Wunner, Phys. Rev. Lett. **74**, 2650 (1995) and Phys. Rev. A **53**, 744 (1996).

[25] T. Pearcey, Philos. Mag. **37**, 311 (1946).

[26] *Handbook of Mathematical Functions*, edited by M. Abramowitz and I. A. Stegun (Dover, New York, 1965).

[27] I. S. Gradshteyn and I. M. Ryzhik, *Table of Integrals, Series, and Products* (Academic, New York, 1965).